



Internship April-July 2014

Hendrik Bosscher
Master student Mechanical Engineering
Engineering Fluid Dynamics
University of Twente

Theoretical and practical approach to improve the film flow of the flywheel experiment

This internship report gives a view on the high velocity droplet impingement in a theoretical and practical way. Theory and practice will come together when droplet impingement will be coupled to the flow qualities of a thin water film.

Contents

- Acknowledgements 4
- List of symbols 5
- Introduction..... 6
- 1. Part A – Droplet impingement 7
 - 1.1. Introduction..... 7
 - 1.2. General theory 7
 - 1.2.1. Sheets 8
 - 1.2.2. Non-Dimensional numbers..... 9
 - 1.2.3. Mapping regimes of droplet impact..... 10
 - 1.3. Experiment 11
 - 1.3.1. Dry surface..... 12
 - 1.3.2. Film 14
 - 1.3.3. Pool..... 15
 - 1.4. Conclusion 18
 - 1.5. Discussion 19
- 2. Part B – flywheel experiment 21
 - 2.1. Introduction..... 21
 - 2.2. Film theory 25
 - 2.2.1. General theory..... 25
 - 2.2.2. Flywheel theory..... 27
 - 2.3. Film improvement 31
 - 2.4. Flywheel experiment part A 35
 - 2.4.1. Set-up 35
 - 2.4.2. Results 39
 - 2.4.3. Discussion 44
 - 2.5. Flywheel experiment part B 50
 - 2.5.1. Set-up 51
 - 2.5.2. Results 53
 - 2.5.3. Discussion 56
- 3. Evaluation and recommendations 58
- References..... 59
- Appendices 61
 - Appendix A 62

Appendix B 67

Acknowledgements

At the end of this internship I would like to thank the people who made it possible to do an internship abroad. I would like to give gratitude to the staff of the Institute of Fluid Mechanics of the Technical University of Braunschweig for having me. Thanks go out to the staff of the Multiphase Flow and Icing department for giving me permission to do the experimental work with their equipment.

I would like to thank my supervisor V. Rohwedder for all the work she did for me and all the support she gave me. Although she had a very busy job she guided me very well. I learned a lot. Also I would like to thank my family for giving me the inspiration to continuously work hard.

List of symbols

Droplet impingement

v_{imp}	Velocity of the droplet at impact m/s
d_D	Diameter of the droplet m
μ_D	Dynamic viscosity of the droplet at 20°C and 1 bar, $kg/m\cdot s$
ρ_D	Density of the droplet at impact at 20°C and 1 bar, kg/m^3
σ_D	Liquid surface tension droplet at 20°C and 1 bar, N/m
V_D	Volume of the droplet m^3
m_D	Mass of the droplet kg

Flywheel experiment

δ	Height of the film m
μ	Dynamic viscosity water $1.0016 \cdot 10^{-3} kg/m\cdot s$
ν	Kinematic viscosity water $1.0016 \cdot 10^{-6} m^2/s$
ρ	Density water $1000 kg/m^3$
σ	Liquid surface tension water $7.2740 \cdot 10^{-2} N/m$
τ_w	Wall shear stress Pa
ω	rotational velocity of the flywheel rad/s
b	Width of the slit m
g	Gravitational acceleration $9.81 m/s^2$
h	Height of the droplet fall m
Q	Volume flow that enters the paddle l/min
r	Radius of the flywheel m
u	Velocity in the boundary layer m/s
y	Coordinate perpendicular to the boundary layer m

Non-dimensional numbers

Re	Reynolds number
Re_{crit}	Critical Reynolds number
We	Weber number
Oh	Ohnesorge number
Ka	Kapitza number

Introduction

This report focuses on the high velocity impingement of water droplets on a thin water surface, a *film*. The Multiphase Flow and icing department of the Institute of Fluid Mechanics in Braunschweig, Germany, currently has its focus on this high velocity impingement of water droplets. A flywheel is being used to reach a high velocity at droplet impact. Here it is possible to capture a droplet impingement on a surface with a thin fluid film with the droplet still being intact at the moment before the impact. To capture a clear image of the droplet impact on a thin fluid film, the film should have some specific properties. The film should be without disturbance to capture the moment of impact. In this report a research is done on both the properties of a droplet impact and on the quality improvement of a thin film. Both subjects don't go without each other in the flywheel research done at the Institute.

Part A of the report focuses only on the different aspects of an impingement of a droplet. Theory will be discussed and a practical approach will be made. Impacts of droplets at different types of surfaces will be captured with a high speed camera. The recordings will be discussed and compared to the available theory. In this part an insight will be created on the qualities that a clear droplet impingement should have and the qualities that a surface should have.

Part B focuses on the high velocity part of the droplet impingement. A continuation of the research done by V. Rohwedder will be done, the high speed droplet impingement on a thin fluid film. The focus will be more on the quality of the thin film than on the droplet impingement. The flywheel used in the foregoing research will be used again. The thin film runs over a surface connected to the flywheel. The rotational speed of the flywheel will be indicated with a non-dimensional number: the Weber number. A goal will be set to reach a high velocity of the flywheel, around a Weber number of 10000, with the thin film still attached to the surface with smooth properties. This goal was not met in the foregoing research of V. Rohwedder. The research will be done with the experimental set-up that was also used in foregoing experiments. Focus will be on the improvement of the film on the surface with the use of a small canal shaped geometry. The canal geometries already designed will be tested again and a literature research will be done to improve these geometries. New designs of the small canals will be made and tested on the flywheel in order to improve the quality of the film.

1. Part A – Droplet impingement

1.1. Introduction

The impingement of droplets on a surface is of wide use in the industry. The use of droplet impingement is important for the finishing of surfaces, for example the painting of cars or the printing on paper, but also in the aerodynamics of airplane wings. In the airplane industry, the impingement of droplets in the air on the wings of airplanes is of much importance. The water film on the airfoil that forms due to the impingement of water droplets can change the aerodynamics of the airplane in ground conditions. Important here is, the arise of *secondary droplets* from a droplet impact. These droplets have a high chance of freezing on the airfoil after impact. Then the iced droplets can detach from the airfoil and fly into the turbo engine. The secondary droplets will be discussed more later. The icing of the water film on airplane wings can cause a change of the lift coefficient and is therefore very dangerous. The change in lift coefficient due to icing makes that the airplane will stall at a lower speed. A view on the impingement of droplets on a surface is therefore very important.

1.2. General theory

The theory focuses on the impingement of a single droplet on a surface. The behavior of the impact of a single droplet depends on a few parameters [1]: The speed of the droplet, the height of the droplet fall, the type of fluid and the type of substrate. For a dry surface the impact reaction depends on the surface roughness of the surface.

Roughly there are a few kinds of droplet impingement on a water film, as can be seen in Fig. 1. The first one is called Reflection. The droplet completely bounces of the water film. This form of droplet impingement only takes place with a low velocity of the droplet. The second type is Coalescence. The droplet is now completely absorbed by the water film. This causes a wave in the water film which dissipates the kinetic energy of the droplet. The third form completely destructs the droplet because of the high impulse of the droplet. The wave of the fluid layer turns into a kind of sheet. From this sheet Secondary droplets will form. This form of impingement is being called Destruction. The reflection is also being called *Bouncing*, the destruction is also called 'Splashing'. The rest of this report focuses on the splashing because it is the most interesting form of droplet impingement for industrial purposes because of the formation of secondary droplets.

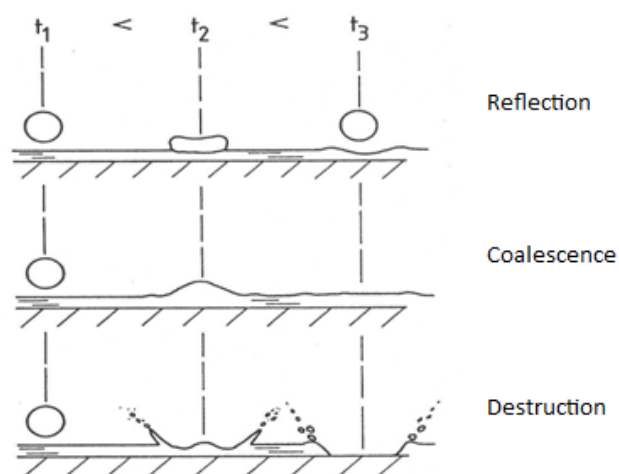


Figure 1: droplet impingement on a water film [2]

A different kind of droplet impingement grouping that is often being used is given below [25]:

- *Prompt splash* High velocity, secondary droplets will originate.
- *Corona splash* The splashing has the shape of a crown.
- *Partial rebound* Part of the droplet bounces back, part disappears in the fluid layer.
- *Rebound* The complete droplet disappears in the fluid layer.

1.2.1. Sheets

The most regular form of splashing of a droplet is a crown. It is the result of a droplet impact with a high impulse on a thin layer of fluid. Harold Edgerton [3] discovered the Milk Drop Coronet, the most regular form of the crown splash formed by a drop of milk. It is formed in the next order of events. A cylindrical wall comes out of the fluid layer. The rim of the cylinder is still flat. Now a linear instability of the rim causes the thickness of the rim to vary periodically. Next tips develop out of the rim. These tips develop into jets which shoot into the air. Then from the end of these jets drops form, as illustrated in Fig. 2. These droplets are the *secondary droplets*.

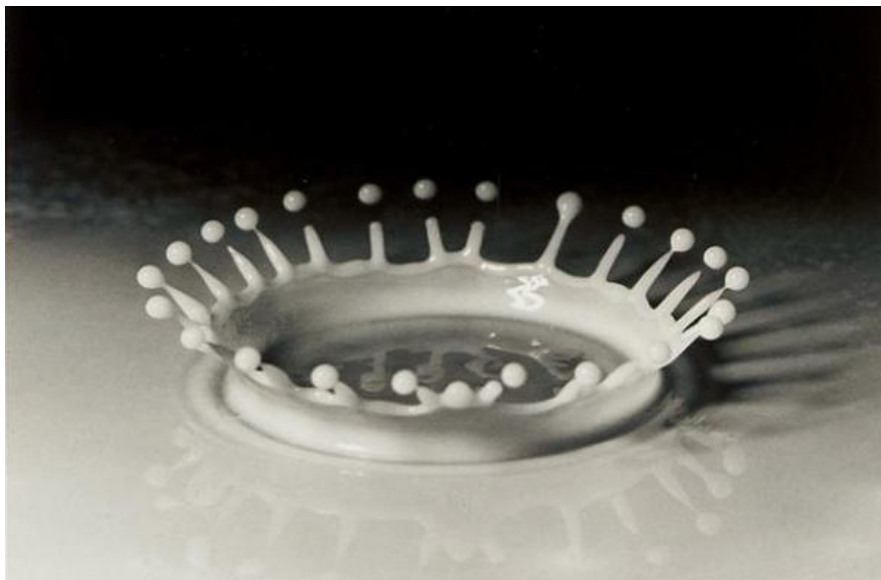


Figure 2: Milk drop Coronet by Harold Edgerton, 1934 [26]

The typically fluid cylinder, or crown, that travels out of the surface is called the *Peregrine sheet*. The Peregrine sheet is first described by Peregrine [4]. The typical crown can be seen in Fig. 3. At position (1) destruction of the droplet at the wall finds place. Splashing occurs and from the water film (6) a sheet forms. In this case the sheet forms a crown (3). From this crown also jets form (4) from which secondary droplets (5) form. These secondary droplets only form when the impulse of the droplet is high enough. Important parameters to define the sheet are the diameter and the height of the crown.

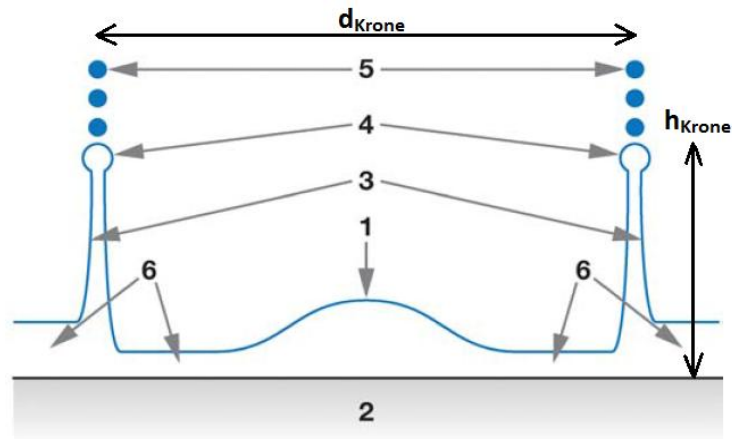


Figure 3: Crown building with splashing [27].

Another type of sheet is the *Ejecta sheet*, first observed experimentally by Thoroddsen [5]. In this type of sheet the fluid is being pushed outward. The fluid layer shoots out horizontally. A picture of an Ejecta sheet can be observed in Fig. 4.

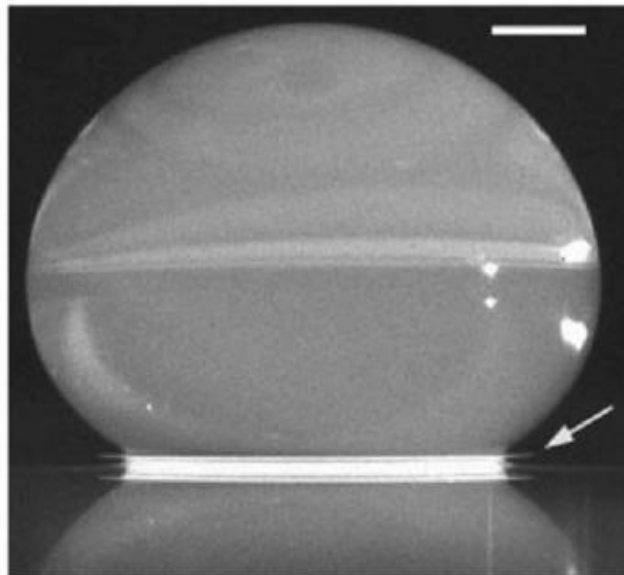


Figure 4: An experimental picture of a drop direct after impact. An Ejecta sheet shoots out horizontally underneath the droplet after impact [5].

1.2.2. Non-Dimensional numbers

The most important parameters to define droplet splashing are the diameter of the droplet and the velocity of the droplet. These parameters can be used to define the conventional dimensionless parameters: The Reynolds number, equation 1.1, and the Weber number, equation 1.2. The Reynolds number is the ratio of inertia forces to viscous forces. The Weber number is defined as the ratio of inertia force to surface tension. Both dimensionless numbers are considered as the most important number to characterize the splashing of a droplet [1]. Both the numbers use the velocity of the droplet at impact, v_{imp} . The Weber number is often used to indicate the velocity of the droplet. A high Weber number means a high droplet velocity.

$$Re = \frac{\rho_D v_{imp} d_D}{\mu_D} = \frac{\frac{kg}{m^3} \frac{m}{s} m}{Pa \cdot s} = \frac{\frac{kg}{m \cdot s}}{\frac{kg}{m \cdot s^2} \cdot s} \quad (1.1)$$

$$We = \frac{\rho_D v_{imp}^2 d_D}{\sigma_D} = \frac{\frac{kg}{m^3} \left(\frac{m}{s}\right)^2 m}{\frac{N}{m}} = \frac{\frac{kg}{s^2}}{\frac{kg \cdot m}{s^2 \cdot m}} \quad (1.2)$$

Also a relationship between the Reynolds and the Weber number is used frequently: the Ohnesorge number.

$$Oh = \frac{\mu_D}{\sqrt{\rho_D d_D \sigma_D}} = \frac{\sqrt{We}}{Re} \quad (1.3)$$

1.2.3. Mapping regimes of droplet impact

In Fig.5 the different regimes of the droplet impacts have been pictured in terms of the Weber number and the Reynolds number. The Crown splash, Peregrine sheet and the arise of secondary droplets have been classified. The picturing of regimes at a higher Weber number has not yet been done.

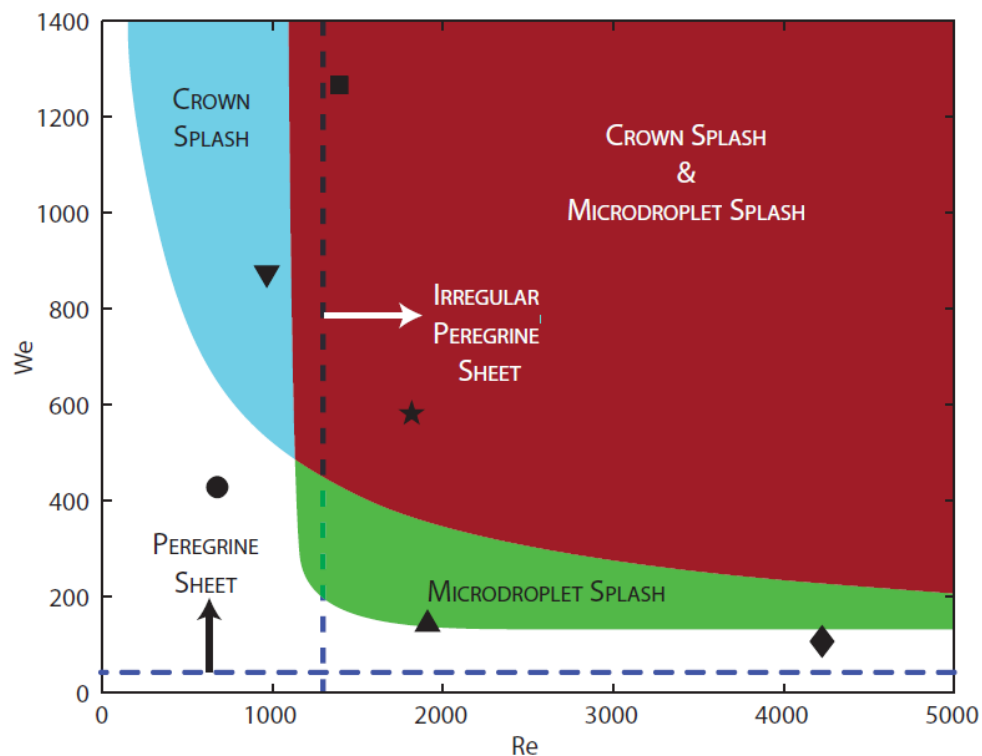


Figure 5: Diagram indicating different regimes of droplet impact for film [1].

1.3. Experiment

To test the theory of the droplet impingement an experiment has been performed. Picturing of the droplet impingement on different surfaces has been made with a high-speed camera¹. The camera is coupled to a computer. Special attention has been placed on the identification of the form of the droplet impingement. There will be an attempt to capture the secondary droplets on camera and identify the different forms of splashing. Different techniques will be used to determine the speed of the droplet and the diameter of the droplet. With these values the Reynolds, Weber and Ohnesorge number can be calculated. With the values of these dimensional numbers known, the kind of impact can be checked with the already known experimentally determined theory: Fig. 5.

For the experiment an aquarium with demineralized water will be used, the droplets from the syringe will also be from demineralized water. Demineralized water is being used because it has a lower mineral content than regular tap water. If regular water evaporates on glass, stains could arise on the glass. This could influence the definition of the pictures. The splashing on the surface will be created with a cuboid made out of Acrylglas. For the lighting of the impact area of the droplet a Halogen light will be used. For the height of the droplet fall two different heights will be tested: 0.24 m and 1.04 m. The droplets will be generated manually with a syringe. The syringe is given height with a construction made out of X95 profiles. The syringe is connected to a plastic tube. The outlet of this tube is positioned to the right position by placing it in a wooden shape. This shape also positions the outlet of the tube in a vertical position. The complete experimental set-up of the height of 1.04 m is pictured schematically in Fig. 6.

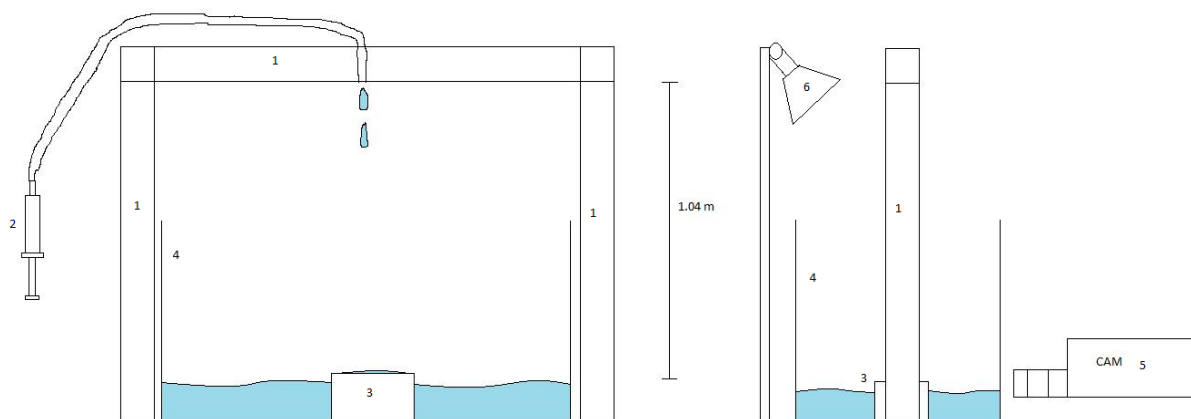


Figure 6: Left: front view experimental set-up, right: side view set-up. 1) X95 profile 2) Syringe 3) Acrylglas Cuboid 4) Aquarium 5) High-speed camera 6) Halogen lamp

The droplet impact will be tested with different surfaces. The cuboid will be used to create a dry surface and a surface with a thin water layer on it. First the surface of the cuboid is smoothed with P2000 sandpaper. The water in the aquarium without the cuboid will be used to create a pool.

To create sharp clear pictures of the droplet impact a few parameters are adjustable. Via the computer the trigger rate and the exposure time of the high-speed camera can be changed. With the trigger rate the amount of pictures taken per time step can be changed, the exposure time is the time of the lighting. On the camera itself the amount of light entering the lens can be changed.

¹ Highspeed camera SpeedSense from the firm Dantec Dynamics

1.3.1. Dry surface

Different recordings were made with different camera settings. Also two different heights have been tested. In Fig. 7 the pictures can be seen for a trigger rate of 200 Hz and an exposure time of 50 μ s. For the lighting here a normal pocket flashlight has been used. The height of the droplet fall is 0.24 m. These settings give a good view on the droplet flying in the air, before the impact. The pictures of the splashing itself are still a bit unclear. To get a better view on the splashing, a higher trigger rate and a higher exposure time have been chosen. The trigger rate is 999 Hz and the exposure time is 1000 μ s. With these adjustments the light source had to be changed. The pocket flashlight was swapped for a Halogen lamp, Fig. 6. Also there was taken a bigger falling height of the droplets, 1.04 m, Fig.6. This gives the results in Fig. 8. Now the form of the splashing is clearly visible.

To calculate the different non-dimensional numbers the diameter of the droplet and the speed of the droplet at impact have to be determined. The size of the droplet can be calculated in two different ways. First an accurate scale was held under the syringe to catch a single droplet. This has been done a few times to minimize the error. From the different weights a mean weight of a droplet is calculated, and also a mean diameter has been calculated from the volume of a sphere. The downside of this method is that it takes the same diameter of the droplet during the whole fall.

$$V_D = \frac{m_D}{\rho_D} = \frac{0.0176 \text{ kg}}{1000 \frac{\text{kg}}{\text{m}^3}} = 1.76 \cdot 10^{-8} \text{ m}^3 \quad (1.4)$$

$$d_D = \sqrt[3]{\frac{6V_D}{\pi}} = \sqrt[3]{\frac{6 \cdot 1.76 \cdot 10^{-8} \text{ m}^3}{\pi}} = 3.2273 \cdot 10^{-3} \text{ m} \quad (1.5)$$

The other method is considered more accurate, the droplet diameter is now determined by the recordings. This method only applies if the droplets are clearly visible on the pictures. The first settings of the camera with the height of 1.04 m have been used to get clear pictures of the droplets. The droplet diameter can now be determined from the recordings right before the impact. This will give a mean droplet diameter of 2.5 mm.

The velocity can be direct calculated from the recordings. The time between two recordings is the exposure time, which is 0.001 s. The height difference right before the impact of the droplet can be exactly determined from two successively recordings. This will give an impact velocity of 2.9 m/s. The three non-dimensional numbers have been calculated for the height of 1.04 m:

$$Re = \frac{\rho_D v_{imp} d_D}{\mu_D} = \frac{1000 \frac{\text{kg}}{\text{m}^3} \cdot 2.9 \frac{\text{m}}{\text{s}} \cdot 2.5 \cdot 10^{-3} \text{ m}}{1.0016 \cdot 10^{-3} \text{ Pa} \cdot \text{s}} = 7238.42 \quad (1.6)$$

$$We = \frac{\rho_D v_{imp}^2 d_D}{\sigma_D} = \frac{1000 \frac{\text{kg}}{\text{m}^3} \cdot (2.9 \frac{\text{m}}{\text{s}})^2 \cdot 2.5 \cdot 10^{-3} \text{ m}}{7.2740 \cdot 10^{-2} \frac{\text{N}}{\text{m}}} = 289.04 \quad (1.7)$$

$$Oh = \frac{\sqrt{We}}{Re} = \frac{\sqrt{289.04}}{7238.42} = 2.35 \cdot 10^{-3} \quad (1.8)$$

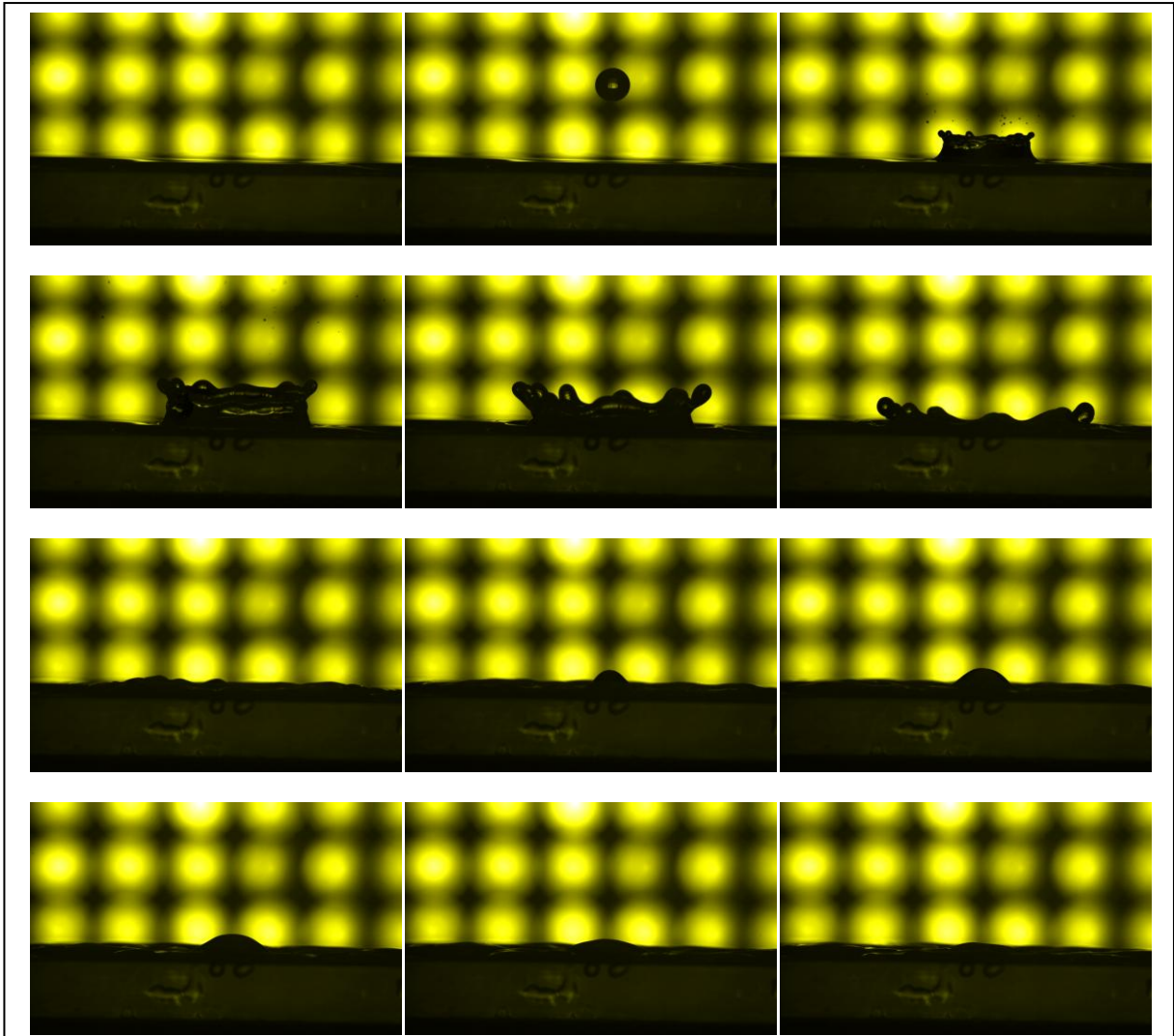


Figure 7: Picture set for dry surface, trigger rate 200 Hz, exposure time 50 μ s, height 0.24 m.

In Fig. 8 a prompt splash can be seen. For a little time a crown forms. The crown completely destruct almost direct after impact. Many secondary droplets have been formed which originate from the crown at high speed.

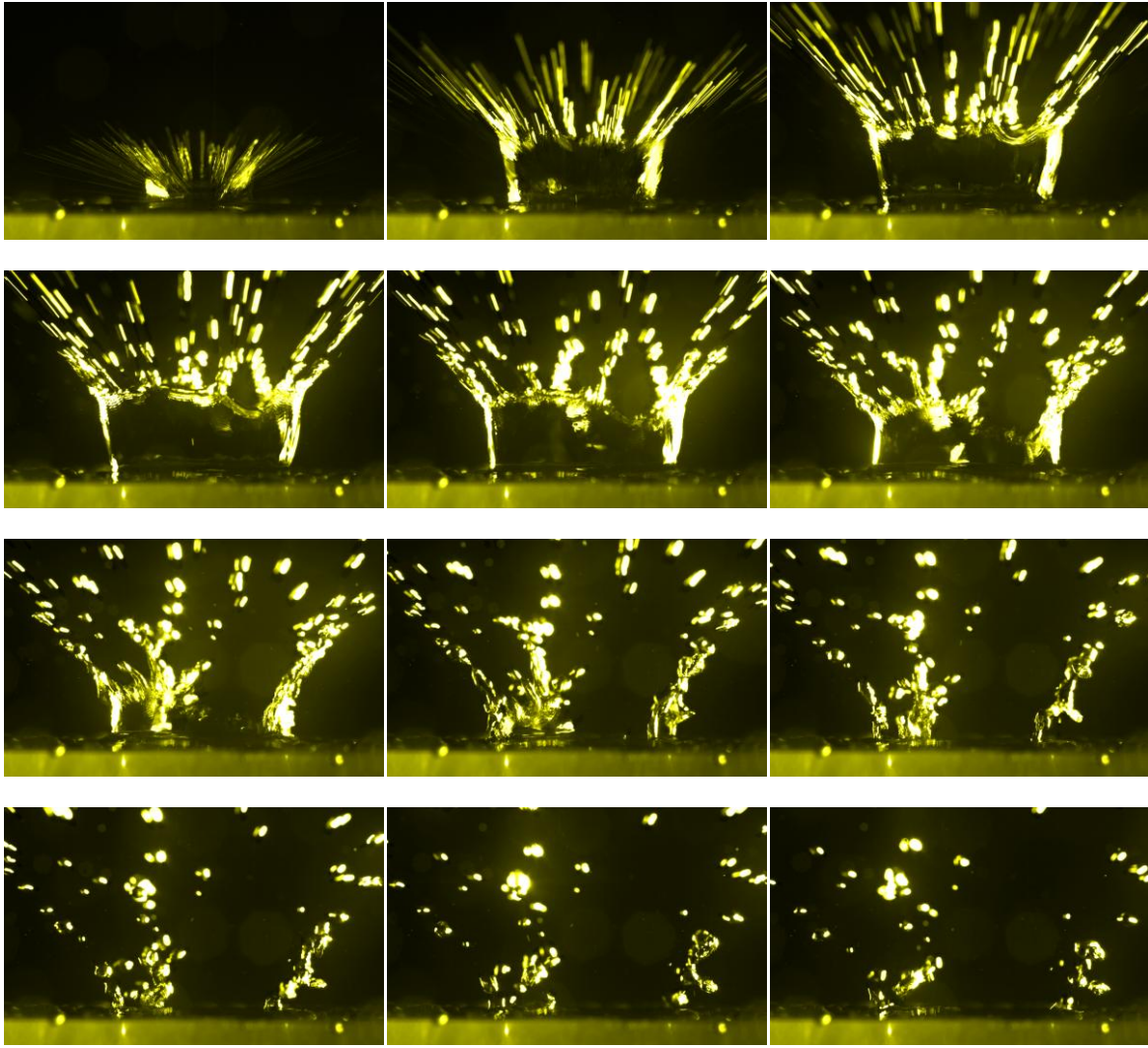


Figure 8: Picture set for dry surface, trigger rate 999 Hz, exposure time 1000 μ s, height 1.04 m.

1.3.2. Film

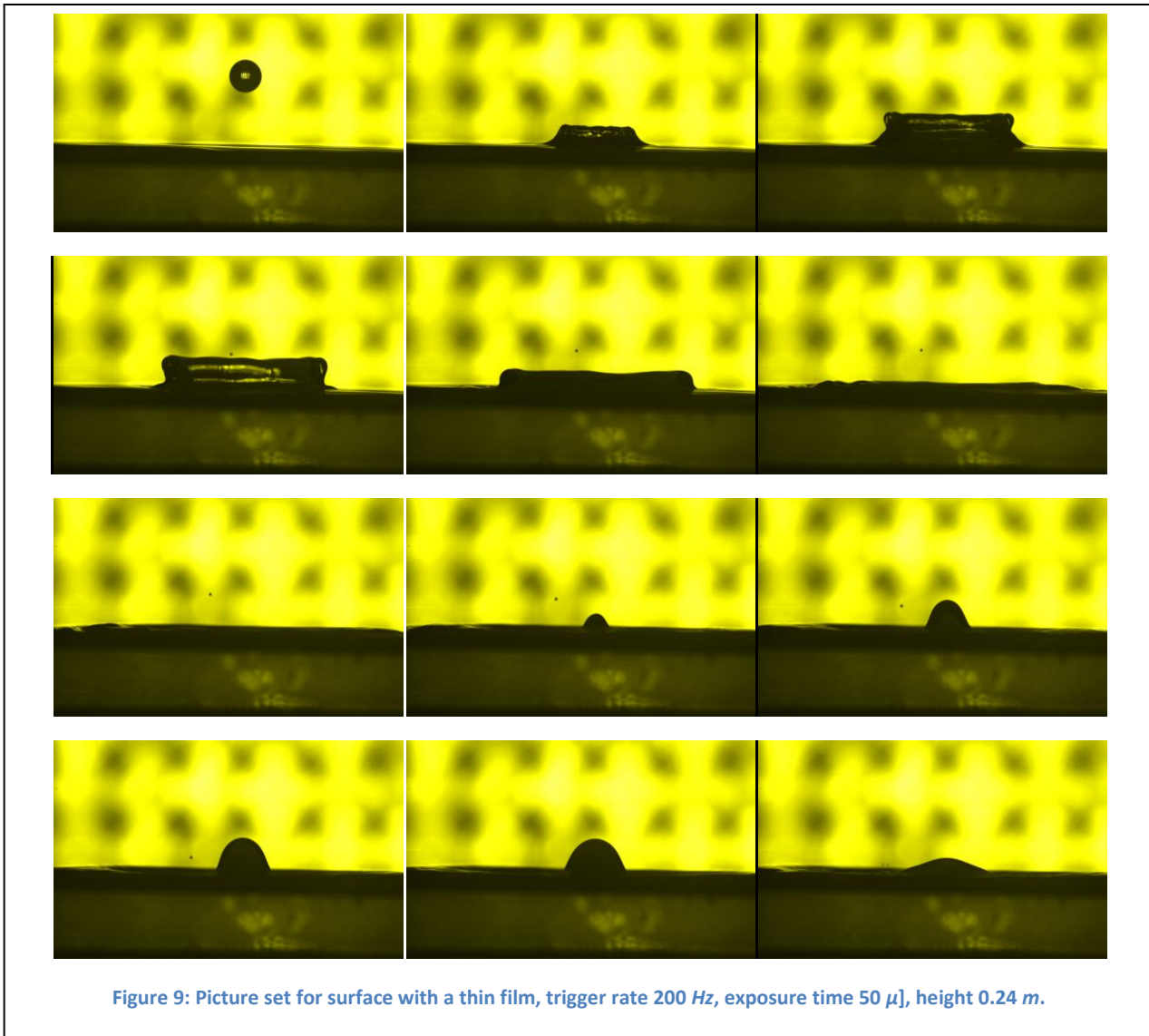
To test the impact on a small water film, the cuboid has been given a tiny film of plus minus 1 mm on top. For the droplet impact on the surface with the thin water film also first the lower height and the other camera settings have been tested. The recordings for the lower height can be viewed in Fig. 9, for the height of 1.04 m in Fig. 10. The pictures determine a droplet diameter of 2.7 mm for the height of 1.04 m and a velocity at impact of 3 m/s. The non-dimensional numbers only have been calculated for the height of 1.04 m.

$$Re = \frac{\rho_D v_{imp} d_D}{\mu_D} = \frac{1000 \frac{kg}{m^3} \cdot 3.0 \frac{m}{s} \cdot 2.7 \cdot 10^{-3} m}{1.0016 \cdot 10^{-3} Pa \cdot s} = 8087.06 \quad (1.9)$$

$$We = \frac{\rho_D v_{imp}^2 d_D}{\sigma_D} = \frac{1000 \frac{kg}{m^3} \cdot (3.0 \frac{m}{s})^2 \cdot 2.7 \cdot 10^{-3} m}{7.2740 \cdot 10^{-2} \frac{N}{m}} = 334.07 \quad (1.10)$$

$$Oh = \frac{\sqrt{We}}{Re} = \frac{\sqrt{289.04}}{7238.42} = 2.26 \cdot 10^{-3} \quad (1.11)$$

The film splashing in Fig. 10 shows a corona splash. The crown that has been formed is clearly visible. The crown originates direct after impact from the thin film and it slowly breaks down. The different lamella from which it is build can also be seen. Secondary droplets have been formed. They originate from the jets that arise from the rim of the crown. The amount of the droplets is clearly less than that of the prompt splashing.



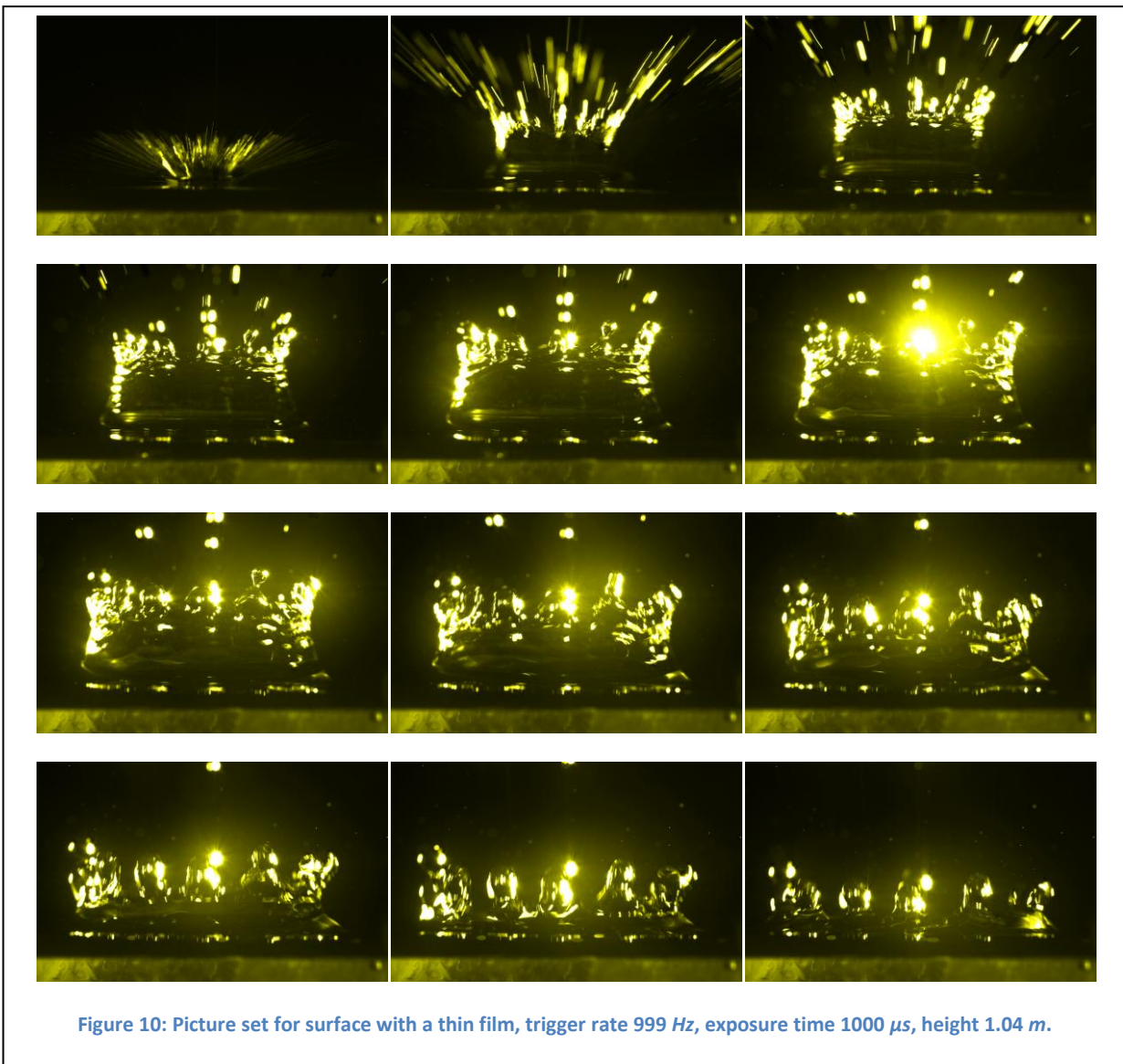
1.3.3. Pool

To test the impact in a pool of demineralized water the cuboid was removed from the aquarium. The recordings of the impact in a water pool are given in Fig. 11 and Fig. 12. The diameter of the droplets turned out to be 2.3 mm and the velocity 2.9 m/s. The non-dimensional numbers for the height of 1.04 m are calculated below.

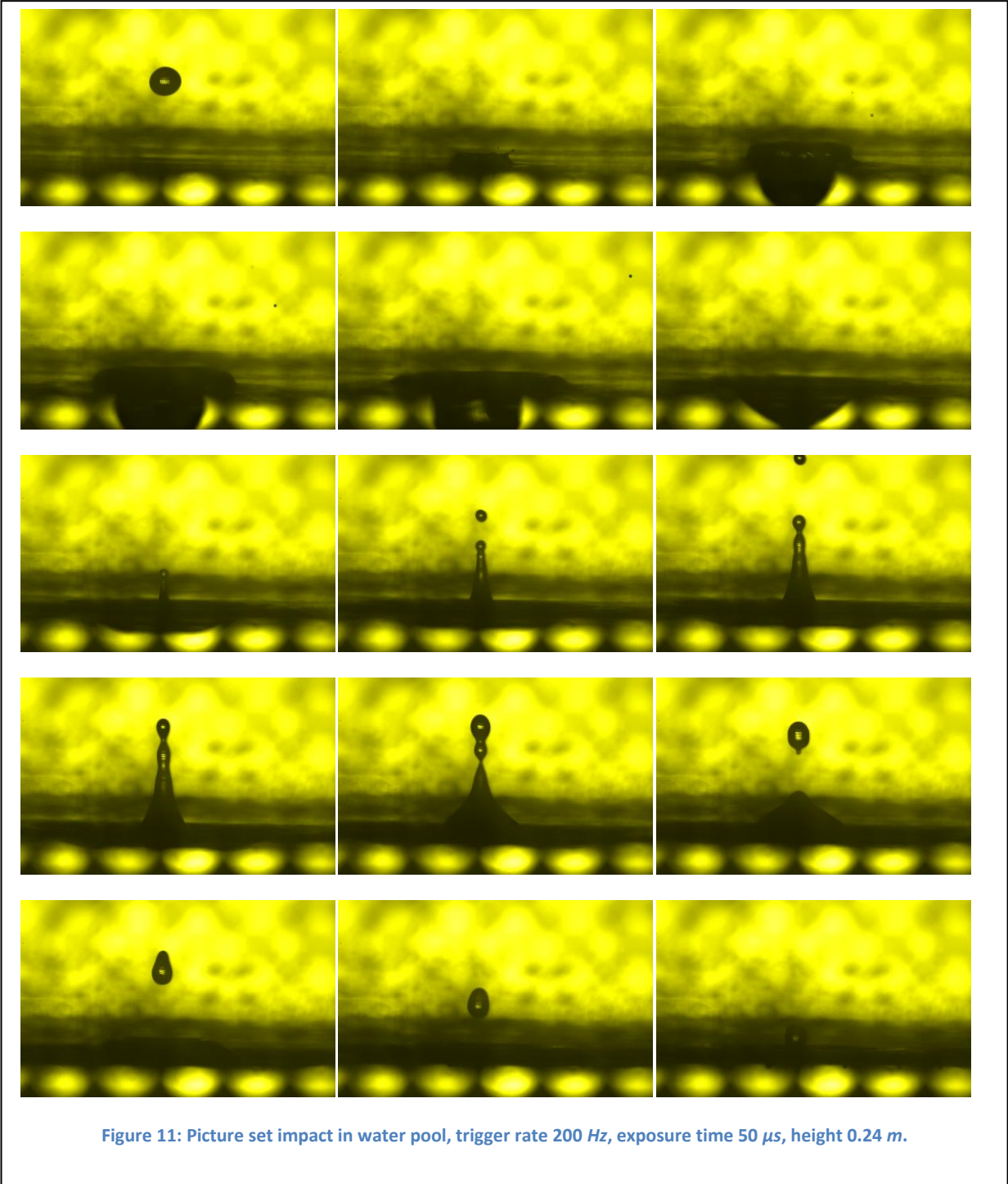
$$Re = \frac{\rho_D v_{imp} d_D}{\mu_D} = \frac{1000 \frac{kg}{m^3} \cdot 2.9 \frac{m}{s} \cdot 2.3 \cdot 10^{-3} m}{1.0016 \cdot 10^{-3} Pa \cdot s} = 6659.35 \quad (1.12)$$

$$We = \frac{\rho_D v_{imp}^2 d_D}{\sigma_D} = \frac{1000 \frac{kg}{m^3} \cdot (2.9 \frac{m}{s})^2 \cdot 2.3 \cdot 10^{-3} m}{7.2740 \cdot 10^{-2} \frac{N}{m}} = 265.92 \quad (1.13)$$

$$Oh = \frac{\sqrt{We}}{Re} = \frac{\sqrt{265.92}}{6659.35} = 2.45 \cdot 10^{-3} \quad (1.14)$$



In Fig. 12 the splashing of a droplet in a water pool can be seen. This is a partial rebound. At the end of the picture series there can be seen that the droplet bounces back from the pool. Part of the droplet stays in the pool and creates a small crown from which secondary droplets form.



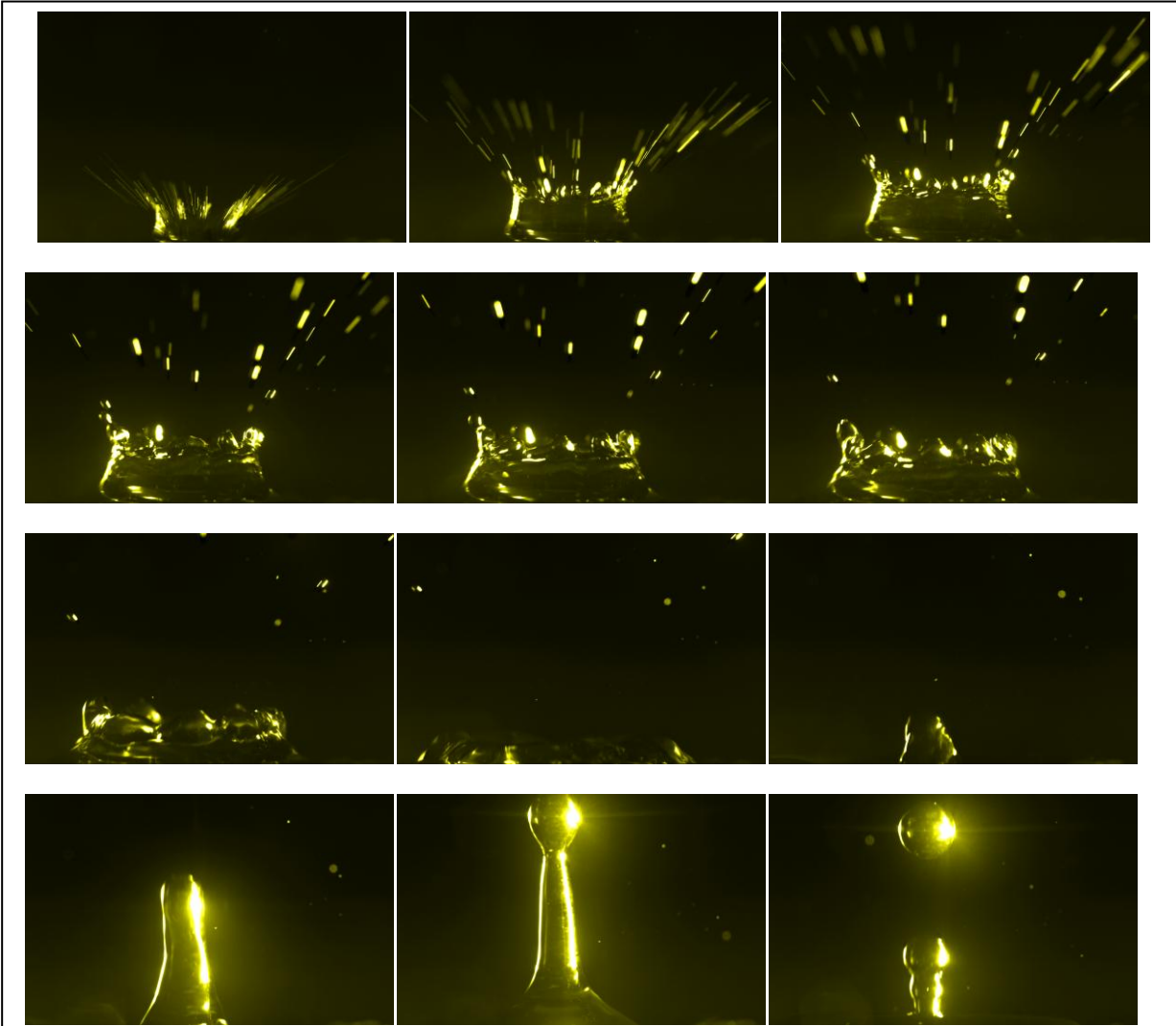


Figure 12: Picture set impact in water pool, trigger rate 999 Hz, exposure time 1000 μ s, height 1.04 m.

1.4. Conclusion

The identification of the different forms of splashing sheets will be done with the recordings of the higher trigger rate of 999 Hz and exposure time of 1000 μ s, and at the bigger height, 1.04 m.

The recordings for the dry surface in Fig. 8 clearly show that the impact of the droplet is of the destruction type. The lamella is visible, which is the primary part of the film after droplet impact. A crown splash is observed with an unstable rim. From this rim a lot of micro droplets eject at high velocity. The crown breaks down and more micro droplets develop. Observed is that the crown doesn't really sink to the bottom but instantaneously breaks up in droplets. This is a sign of a *prompt splash*, which is observed at high velocities and high impulses.

For the impact of a droplet on a thin film clearly a Crown splash is observed, Fig. 10. Instantaneously after impact a crown ejects almost vertically from the film. Jets evolve from the irregular rim and from these jets secondary droplets develop. The size of the secondary droplets is bigger than those of the dry surface splash. The crown then becomes less high and goes back into the film. The lamellas

that form the crown are clearly visible in the middle of the picture set. The jets from which the secondary droplets develop stay visible during the whole splash.

The picture set of the impact in the pool is observed in Fig. 12. Here also a crown splash forms upon impact. Observed is, that the crown is lower than that of the other film and that of the dry surface crown. Here also secondary droplets form which are just as for the dry surface splash very small. The crown clearly shows the different layers of lamellas from which it is built. Just as for the film splash the height of the crown becomes smaller and smaller and the crown disappears in the pool. At a certain time step a jet appears from the pool from which a big secondary droplet develops. Both disappear in the pool. The big secondary droplet creates small waves in the pool.

In table 1 a recap has been given of the non-dimensional numbers for the different impacts.

	<i>Re</i>	<i>We</i>	<i>Oh</i>
<i>Dry</i>	7238.42	289.04	$2.35 \cdot 10^{-3}$
<i>Film</i>	8087.06	334.07	$2.26 \cdot 10^{-3}$
<i>Pool</i>	6659.35	265.92	$2.45 \cdot 10^{-3}$

table 1: Non-Dimensional numbers droplet impact

1.5. Discussion

With the non-dimensional numbers being known, table 1, the appearance of splashing can be compared with the theory [6], for impact on a dry surface and for impact on a thin film. In this research the authors investigate different fluid impingements and come up with a relation for the splashing boundary. The splashing boundary for impact on a dry surface can be seen in Fig. 13.

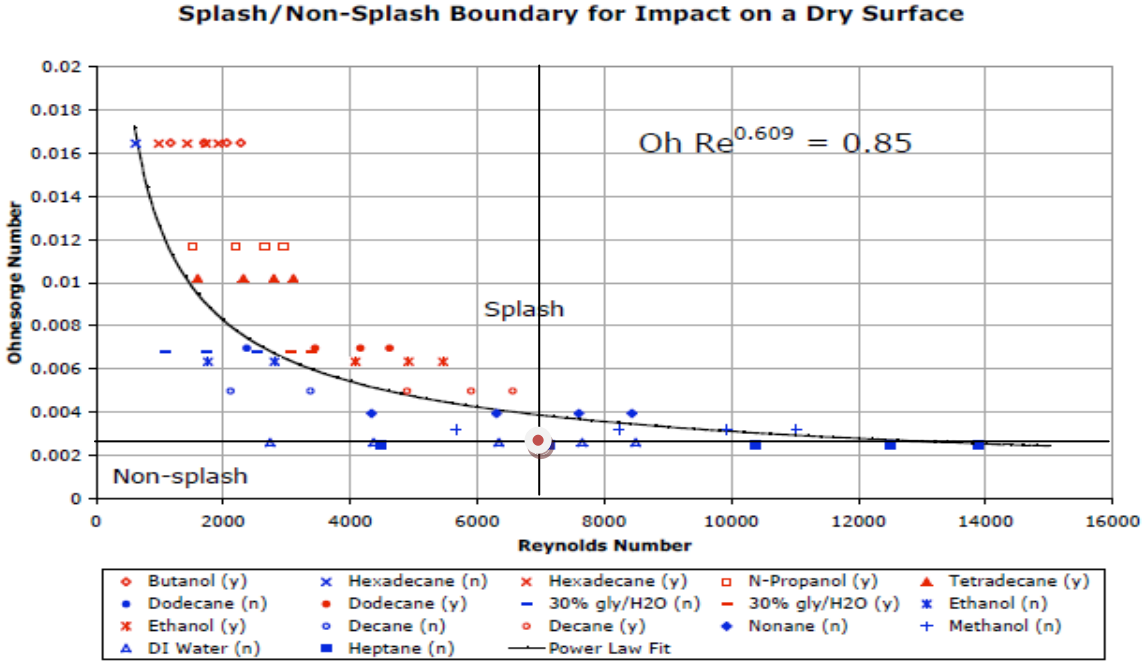


Figure 13: Splashing boundary for impact on a dry surface [6].

The experimental results have been pointed out in the figure by a red dot. For the impact on a dry surface the results don't correspond with the theory from Vander Wal. For the impact on a thin film, Fig. 14, the results do correspond.

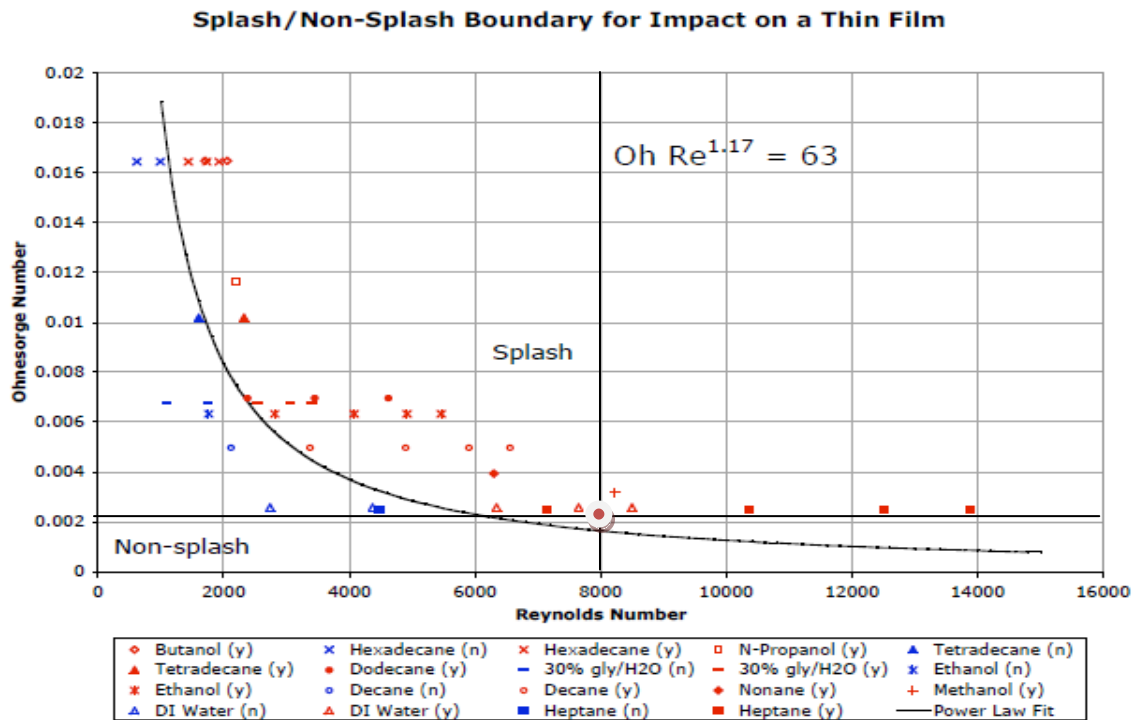


Figure 14: Splashing boundary for impact on a thin film [6].

The reason that the results of the dry surface experiment don't correspond with the theory is probably inaccuracy. The droplets were dropped with a syringe on the dry glass cuboid. The cuboid surface was dried every time an experiment had been done. But the pictures taken weren't always from the first drop to hit the surface. This means that a few drops already were on the surface when the pictures were taken. This causes the inaccuracy of the results. The results for the dry surface depend very much on the surface roughness of the cuboid surface. The surface of the cuboid has been edited with P2000 sandpaper until a smooth surface was created. The amount of splashing depends on the amount of sanding that has been done. For the splashing on a thin film it is easier to create a good result because most of the time a small film was present on the surface. This type of splashing also depends on the surface conditions, hence on the thickness of the film present. A thinner film will create a splashing that is more like a pool splashing. And a thicker film will create a splashing that is more like a pool splashing.

2. Part B – flywheel experiment

2.1. Introduction

The second part of this report focuses on film flow on a flat surface. Currently the Institute of Fluid Mechanics in Braunschweig, Germany, is occupied with the research of high velocity droplet impingement of a water droplet on a water film. In the introduction of Part A the importance of droplet impingement on surfaces already was explained. Some of the applications of droplet impingement, for example an airplane at a height of 2 km, require a high speed droplet impingement. The easiest way to test this high velocity droplet impingement is to let a droplet fall from a big height. The droplet will however not have the same shape at the bottom as at the top, as a matter affect the droplet will completely fall apart because of the high velocity. To test the impact of a droplet at high velocity, hence at high Weber number, W . Faßmann et. al. designed a flywheel [7]. On the lateral area of the flywheel a surface has been attached. A smooth Quartz glass plate has been chosen as the surface. The length of the surface is directed in radial direction. The droplets will hit the surface at free falling conditions when the wheel is spinning. In this way there will be a high velocity droplet impingement on a surface with the droplets still in their original form. The experimental set-up as designed by Faßmann can be seen in Fig. 15.

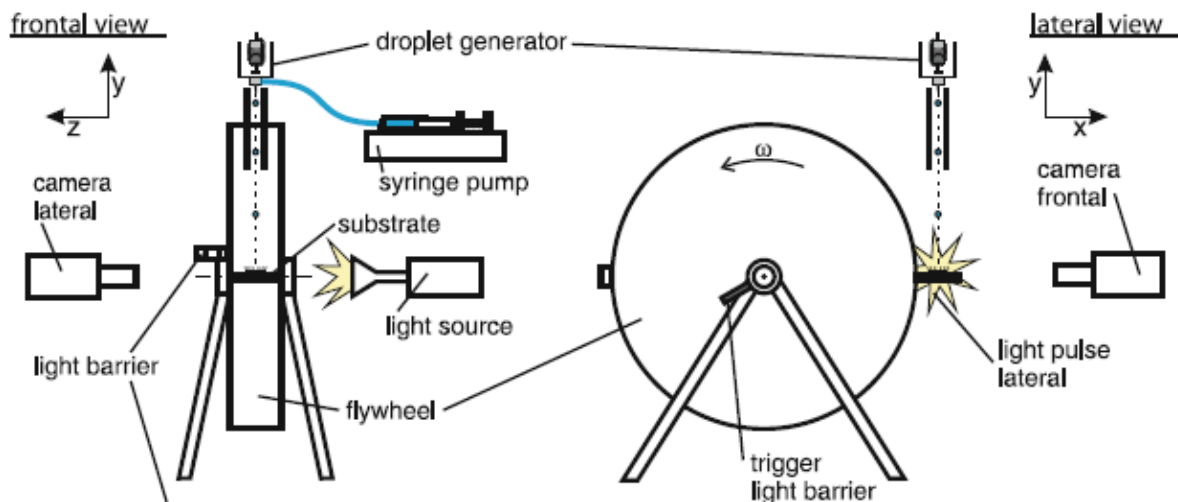


Figure 15: Experimental set-up by faßmann [7].

The flywheel rotates at constant velocity. Via the droplet generator droplets will fall on the glass plate. The light barrier will cause the droplet generator and the high velocity camera to function at the right time. At this moment also a light pulse will be given by the laser, which has been used as light source [7]. The research of V. Rohwedder [28] and also the experimental work in this report are based on this set-up. A more detailed version of the set-up will be given in section 2.4.

To test the impact of droplets at high Weber number on a surface with a thin film, W. Faßmann designed a paddle, Fig. 16, which is currently still being used for research at the Institute in Braunschweig. The paddle can be attached at the lateral side of the flywheel. From this flywheel, water runs into the rectangular inlet of the paddle seen in the right picture of Fig. 16. Through a convergent Aluminium canal the water runs through a slit on the Quartz glass plate.

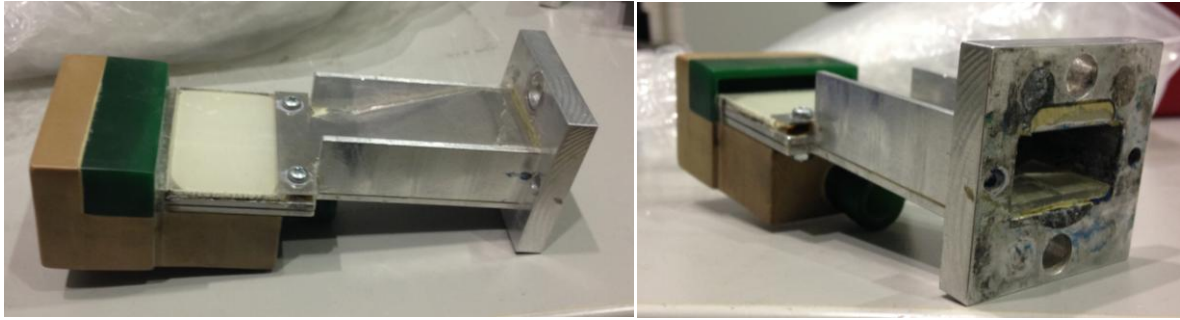


Figure 16: Paddle with glass plate designed by W. Faßmann.

The height of the slit can be adjusted by the two screws, the width of the slit is not adjustable. A maximal slit height of circa 0.3 mm can be achieved. The flow of water through the slit will form a thin film on the glass plate. At the back of the paddle an outlet has been created. Under this outlet a hose has been attached which is attached to the flywheel. The flywheel has two water connections. The first is with a hose connected to the inlet of the paddle. The second is connected with the outlet of the paddle to carry off the water from the thin film. A more detailed description of the further water circuit will be given in section 2.4.

With this paddle from Faßmann a Weber number of the droplet of 6000 could be achieved, for the droplet impingement case on a water film. If the velocity of the droplets, hence the velocity of the flywheel, became higher the film on the paddle ripped open or became detached from the glass plate. In this way research of the high velocity droplet impingement on a thin water film wasn't possible. The work of V. Rohwedder was a continuation of the research of Faßmann. The goal was to get a better estimation of the influences on the thin film flow. With the understanding of these influences a better film and thus a better view on the droplet impingement would be achievable. The thickness of the film and the velocity of the film should be adjustable independent of each other. To realize this V. Rohwedder designed a new paddle that was also applicable on the flywheel, Fig. 17.

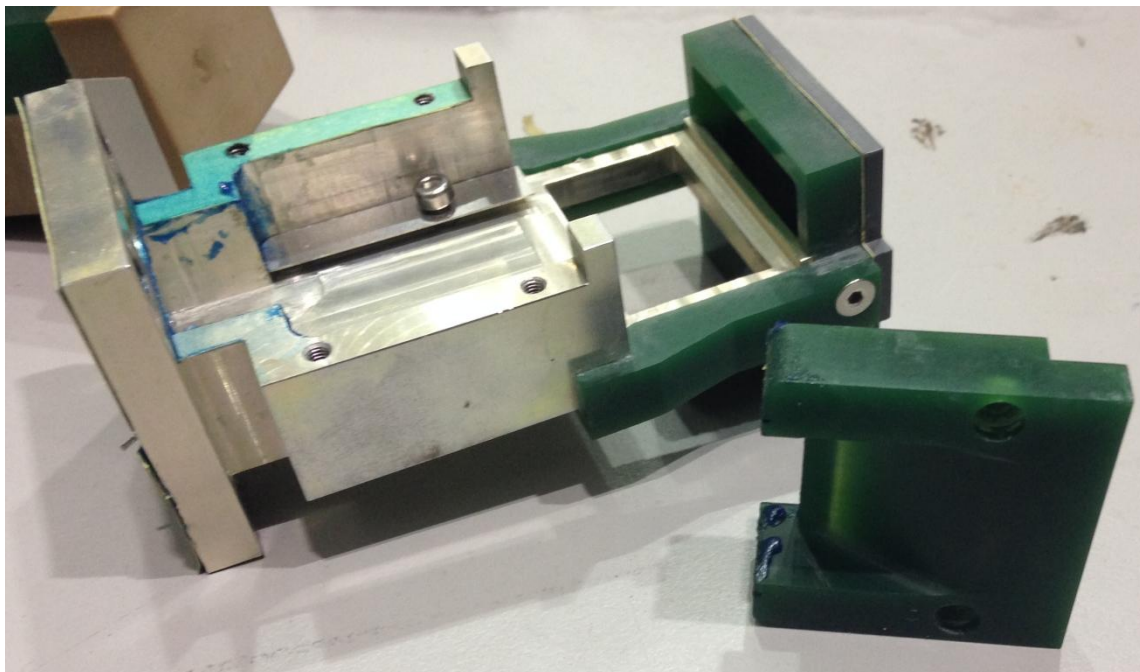


Figure 17: New paddle designed by V. Rohwedder

The new paddle consists out of different parts. With this modular construction a better insight can be given on the exact influences on the thin film and the flow instability of this film. The old paddle is not demountable and only the height of the slit could be adjusted to a certain value.

The paddle of V. Rohwedder consists mainly out of an Aluminum part, Fig. 17. This part of the paddle is attached to the flywheel with four screws. The plate made out of Quartz glass is placed in the Aluminum housing. The outlet is attached to the Aluminum housing with stainless steel screws. The shape of the canal through which the water runs is now defined by an individual part, a *geometry* or *film lip*. A view of such a geometry can be seen in Fig. 17 and Fig. 20. The changing of the height difference of the slit will be done with the use of thin stainless steel plates. The plates can be put in the Aluminum housing and will be tightened with screws to the glass plate. Therefore two holes have been made in the glass plate. In Fig. 18 two of these plates with a height of 0.2 mm can be seen. On top of these plates the geometry from Fig. 20 is placed.

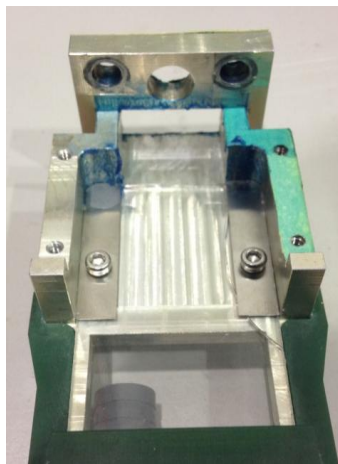


Figure 18: Stainless steel plates attached to the paddle.

In Fig. 19 two forms of these plates can be seen. With the wider plate, the right one in Fig. 19, a slit width of 14 mm can be realized, the other plate will give a width of 24 mm. The plate at the right side in Fig. 19 is shaped according to the so called Börger-Curve.

The canal shaped geometry that has been designed by V. Rohwedder can be seen in Fig. 20, on the left. The shape of this geometry has also been chosen according to the Börger-Curve [28], the optimal contour that is used in wind tunnel designs. This contour is used for the roof of the canal. The end of the roof of the canal has been made straight, in order to calm down the flow [28]. The sides are straight and the bottom is the glass plate. The canal shaped geometry fits in the Aluminum housing and presses on the two stainless steel plates on the glass plate. It is thereby very important that the canal shaped geometry will fit tight in the housing to prevent leakage through thin slits. Also it is important that the canal shaped geometry will fit tight onto the two plates to prevent an additional flow under the plates. Also a second geometry has been made, visible on the right side of Fig. 20. This shape is based on the convergent shape of the paddle designed by Faßmann. The sides of this canal are straight, the roof has an angle of 23.08° with the glass plate. The end of the roof is again straight. The sides of this last straight end will thus be formed by the two stainless steel plates.

Both the geometries will fit tight in the housing. The canal shaped geometry will thereby be pressed onto the two plates by the use of an Aluminum plate. The method can be seen in Fig. 21.

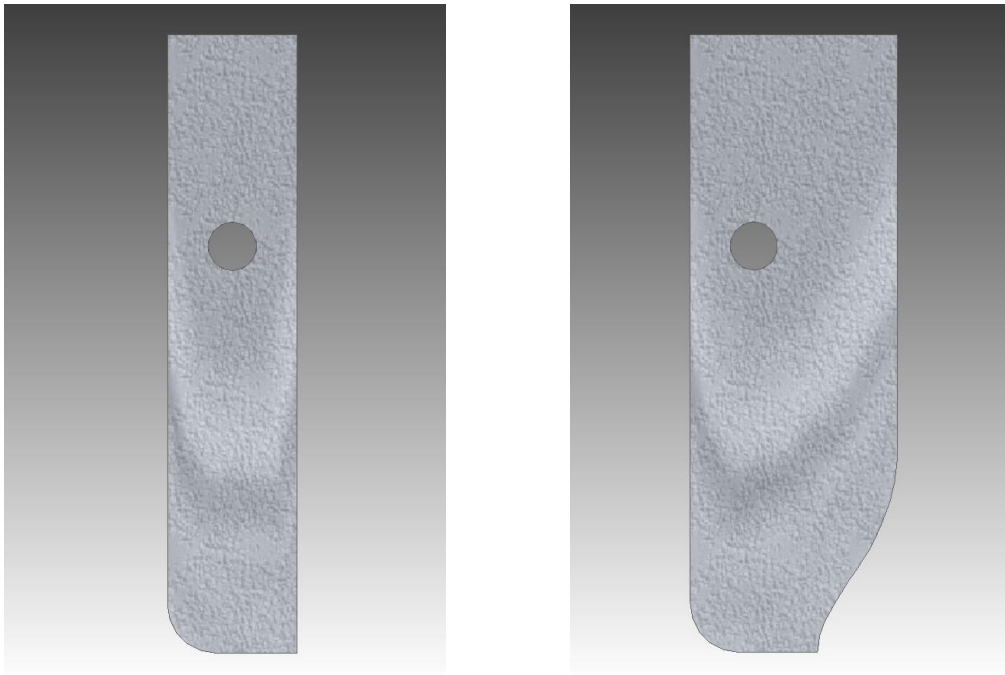


Figure 19: Two different stainless steel plates to realize a slit width of respectively 24 mm and 14 mm [28].

The u-shape on top of the geometry will fit in the u-slit in the Aluminum plate. The Aluminum cover will fit tight on top of the housing. It is important that the different pieces form a waterproof closure. To achieve this, different methods will be applied. These methods will be clarified in the experimental section: Section 2.4.



Figure 20: Canal shaped geometry designed by V. Rohwedder [28] on the left, geometry based on Faßmann [7] on the right.

The two canal shaped geometries have been produced by means of CNC milling, in which CNC stands for *Computer Numerical Control*. The material from which the canal shaped geometry as well as the outlet part has been constructed is Necuron® 702 [28]. This material is well known because of its good processing abilities.

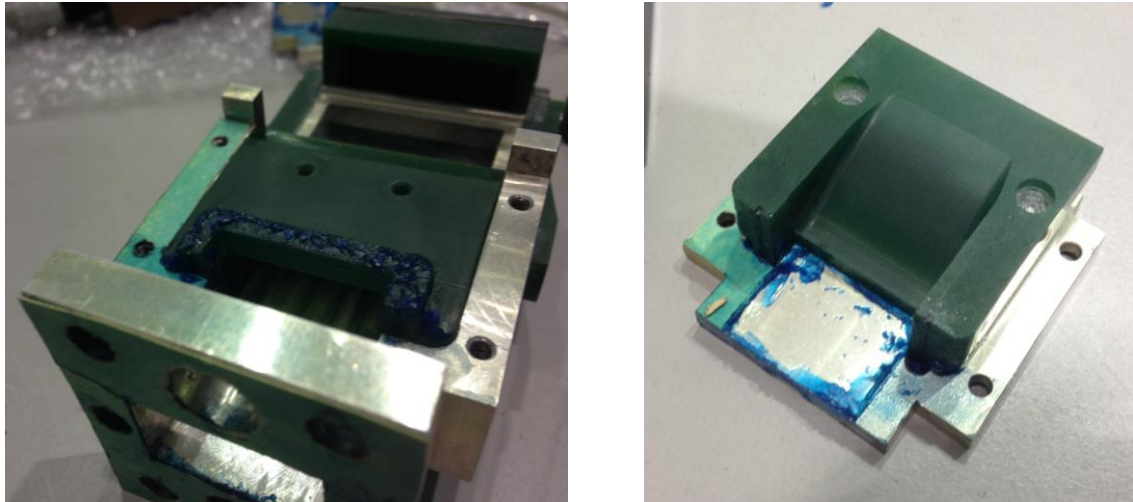


Figure 21: Stainless steel plates attached to the paddle.

Goals:

The first goal of this report is to determine the relation between the two non-dimensional numbers, Reynolds and Weber, and the height of the film. V. Rohwedder determined in her research the Reynolds and the Weber number dependent of the variables used in the flywheel experiment [28]. The goal is to combine these numbers with the relationship for the film height so that easily for different film heights the working area can be determined in terms of the Reynolds- and Weber number.

The second goal of this report is to research the influence of the geometry of the canal on the stability of the thin film. V. Rohwedder did tests on the canal shaped geometry that she designed herself, the left one in Fig. 20, for a slit height of 0.1 mm and 0.3 mm [28]. Her goal was to reach a Weber number of 10000. However detachment of the film flow occurred at a Weber number of 5826 for a slit height of 0.1 mm and at Weber number of 5106 for a slit height of 0.3 mm. The occurrence of turbulence at the surface of the film was visible at this point [28]. The goal of this report will be the development of a new canal shaped geometry. With this new geometry a smooth film at a higher rotational speed of the flywheel, hence Weber number, should be reached. The film should stay attached to the glass plate with as low turbulence in the flow as possible. Eventually the goal is to reach a Weber number of 10000. For the testing of the new geometries a set-up based on the set-up from Rohwedder and Faßmann will be used, Fig. 15. Because the focus in this report is on the film flow on the paddle, the droplet impingement on the paddle will not be tested. To compare the new designed geometries, the two geometries made by Rohwedder, Fig. 20, as well as the old paddle from Faßmann will also be tested. Regarding the two kind of plates, only the smaller plates will be used. Hence the plates will be used that lead to a slit with a width of 24 mm. This will be further explained in the experimental section: section 2.4.

2.2. Film theory

2.2.1. General theory

In this report the thin flow of water over a flat surface is considered. The flow that we are dealing with is thus an incompressible viscous flow. Here a small review of the boundary layer theorem will

be given. The difference between laminar and turbulent flow will be repeated, the difference will be important in the experiments that will follow in this report. The thin viscous region near a body adjacent to the flow is called the boundary layer. Fig. 51 gives the velocity profile for a boundary layer over a flat plate. The velocity starts at a value of zero at the surface and continuously grows to a value of V at the outer edge of the boundary layer. Each boundary layer has also a temperature profile but this is not important for this report. The slope of the velocity profile at the wall is important because it defines the wall shear stress:

$$\tau_w = \mu \left(\frac{dV}{dy} \right)_{y=0} \tag{2.1}$$

In which y is the coordinate that runs perpendicular from the surface. μ varies with the temperature, for liquids μ decreases as the temperature increases.

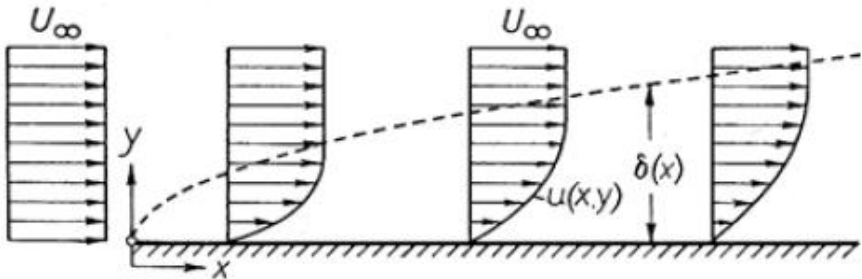


Figure 51: Velocity profile for flow over a flat plate [8]

In general there are two types of viscous flow exist: laminar flow and turbulent flow. In laminar flow the streamlines are smooth and fluid elements move smoothly along the streamlines. In turbulent flows the streamlines are not smooth anymore. Fluid elements move in a random irregular way. The transition between the laminar and turbulent areas of a flow is indicated by a critical Reynolds number. The velocity that has been used in this Reynolds number is the mean velocity in the boundary layer. O. Reynolds has shown the laminar and turbulent behavior of a water flow (1883) [8]. Reynolds made the behavior of the flow clear by putting a colored fluid in the water stream. The result has been given in Fig. 52.

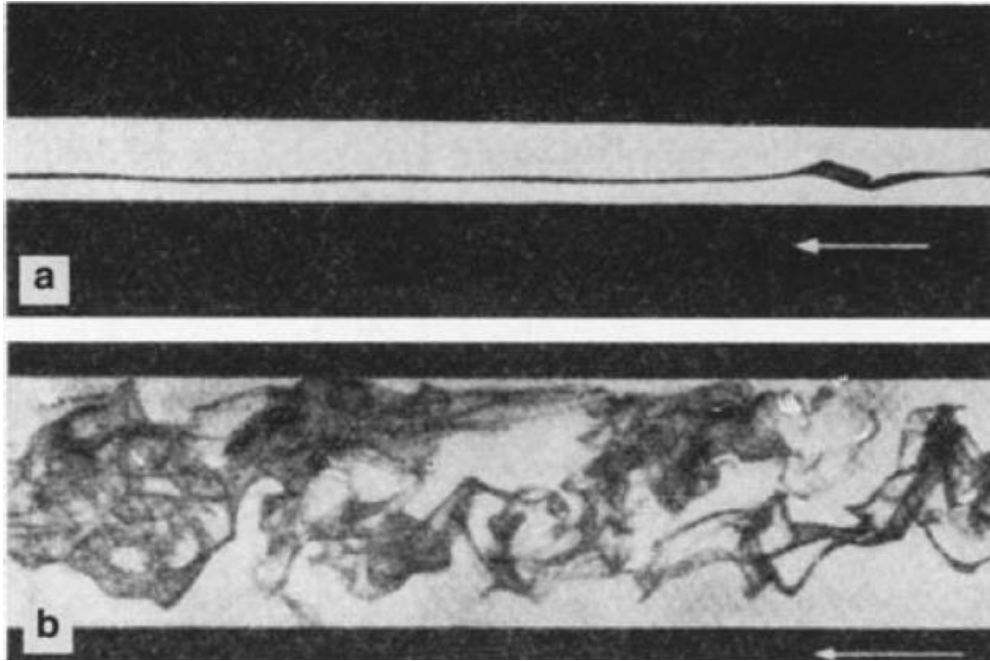


Figure 52: Laminar and Turbulent flow by Reynolds [8]

In picture *a* can be seen that a fluid thread has developed which runs parallel to the canal. In this flow, the laminar flow, fluid layers of different velocities run next to each other without the exchange of fluid parts in perpendicular direction. If the velocity of the flow is increased beyond the critical Reynolds number, the flow becomes turbulent. See Fig. 52 *b*. In the flow the colored threads now run in a disordered fashion. The strings now run also in the perpendicular direction. There are many fluctuations in the flow. [8] [29]

2.2.2. Flywheel theory

To fully describe the theory of the flywheel experiment V. Rohwedder described a few relations. The relations are dependent on parameters used in the flywheel experiment. To describe this theory also the impingement of the droplet on the paddle has to be taken in account. A relation for the film height or boundary layer thickness, on the rotating paddle has been described by V. Rohwedder, equation 2.2 [28]. The film height is according to this relation dependent on different parameters:

- Flywheel parameters: ω : rotational speed of the flywheel, r : radius of the flywheel, Q : volume flow that enters the paddle, φ : phase angle of the paddle with respect to the vertical position.
- Paddle parameters: b : width of the slit.
- Fluid parameters: μ : dynamic viscosity of water, ρ : density of water.
- Other: g : gravitational acceleration.

In this relation the centrifugal force, due to the rotation of the flywheel, and the gravitational force have been described. Because most of the theory of film flow is for falling films there has been chosen to work with the equation for a vertical position of the paddle, equation 2.3.

$$\delta = \sqrt[3]{\frac{3\mu Q}{b\rho(r\omega^2 + g \sin \varphi)}} \quad (2.2)$$

$$\delta = \sqrt[3]{\frac{3\mu Q}{b\rho(r\omega^2 + g)}} \quad (2.3)$$

Also the two important non-dimensional numbers, the Reynolds- and the Weber number have been rewritten with respect to the parameters of the experiment. The Reynolds number, equation 2.4, has only parameters from the flywheel and the fluid in it.

$$Re = \frac{Q\rho}{b\mu} \quad (2.4)$$

The relation of the Weber number, equation 2.5 [28], introduces the parameters of the droplet: h , the height of the droplet fall; d , the diameter of the droplet. The surface tension of the droplet, σ , and the density of the droplet, ρ , are assumed to be the same as for water.

$$We = \frac{\rho(\sqrt{2gh} + r\omega)^2 d}{\sigma} \quad (2.5)$$

The Weber number only has parameters from the fluid, water, and the droplet in it.

There has been tried to rewrite the Reynolds- and the Weber number both as function of both omega and the flow rate. However as told before, according to the theory from V. Rohwedder, the two non-dimensional numbers are only a function of these individual variables. The characteristics of the two non-dimensional numbers are thus straight lines. Literature research has been done to find another way to relate the Reynolds- and the Weber number to both the rotational speed and the volume flow. F. Dietze describes the velocity profile for a vertically falling film [9]:

$$u(y) = \frac{g\delta^2}{2\nu} \left[2\frac{y}{\delta} - \left(\frac{y}{\delta}\right)^2 \right] \quad (2.6)$$

A. Alhelfi describes the velocity profile over a rotating disk [10]:

$$u = \frac{\omega^2 r \delta^2}{2\nu} \left[2\frac{y}{\delta} - \left(\frac{y}{\delta}\right)^2 \right] \quad (2.7)$$

The combination of these two equations, the falling and the rotating part, lead exactly to the velocity profile for a falling rotating film in the research of V. Rohwedder [11]. Integration of this velocity profile over the boundary layer and rewriting to delta will lead to equation 2.3. There can thus be assumed that the way of V. Rohwedder is the right one and that there is simply no way of expressing Reynolds and Weber in both the rotational speed and the volume flow.

The only way to map the important areas of the Reynolds- and the Weber number is thus with the straight characteristics. In Fig. 22 the Reynolds- and Weber number and the film height have been plotted. Only the film height is dependent on both the rotational speed and the volume flow. With this diagram it is now easy to determine the right working area in the flywheel experiment. When a specific Weber number and Reynolds number are preferable, the right slit height can be determined from the diagram. In the diagram the Weber characteristics for the values of 3500 and 5000 have been especially displayed because between these two values most of the literature is available.

Hartley and Murgatroyd [12] came up with the following relation for a critical Reynolds number:

$$Re_{crit} = 1.70 \cdot (1 - \cos \theta)^{\frac{3}{5}} \cdot K_f^{\frac{1}{5}} \quad (2.8)$$

Here is θ the contact angle in a three-phase system. For the case of the experiment the angle is for water on glass. According to [13] the contact angle for water and glass can be assumed to be 15° . K_f is a number that involves the *Kapitza number*, a non-dimensional number that relates the surface tension to the viscosity [14].

$$K_f = Ka^3 = \frac{\sigma^3 \rho}{g \mu^4} \quad (2.9)$$

For water at 20°C and at 1 bar , K_f gives a value of $3.891 \cdot 10^{10}$ [15]. Now the critical Reynolds number follows from:

$$Re_{crit} = 1.70 \cdot (1 - \cos 15^\circ)^{\frac{3}{5}} \cdot (3.891 \cdot 10^{10})^{\frac{1}{5}} = 313 \quad (2.10)$$

This gives a theoretical value for the maximal allowed Reynolds number. After this number the film will become unstable. With this value for the Reynolds number and the value of 10000 for the Weber number a specific area in the diagram could be indicated. Hence the area in the diagram could be indicated for which the film flow should stay attached to the paddle. With a specific rotational speed know beforehand this area could be indicated. In this way it is possible to compare the outcome of the experiment with the theoretical outcome. If the film flow separates from the glass plate at a certain film height and Weber number this could be compared with the theory by means of the diagram in [Fig. 22](#).

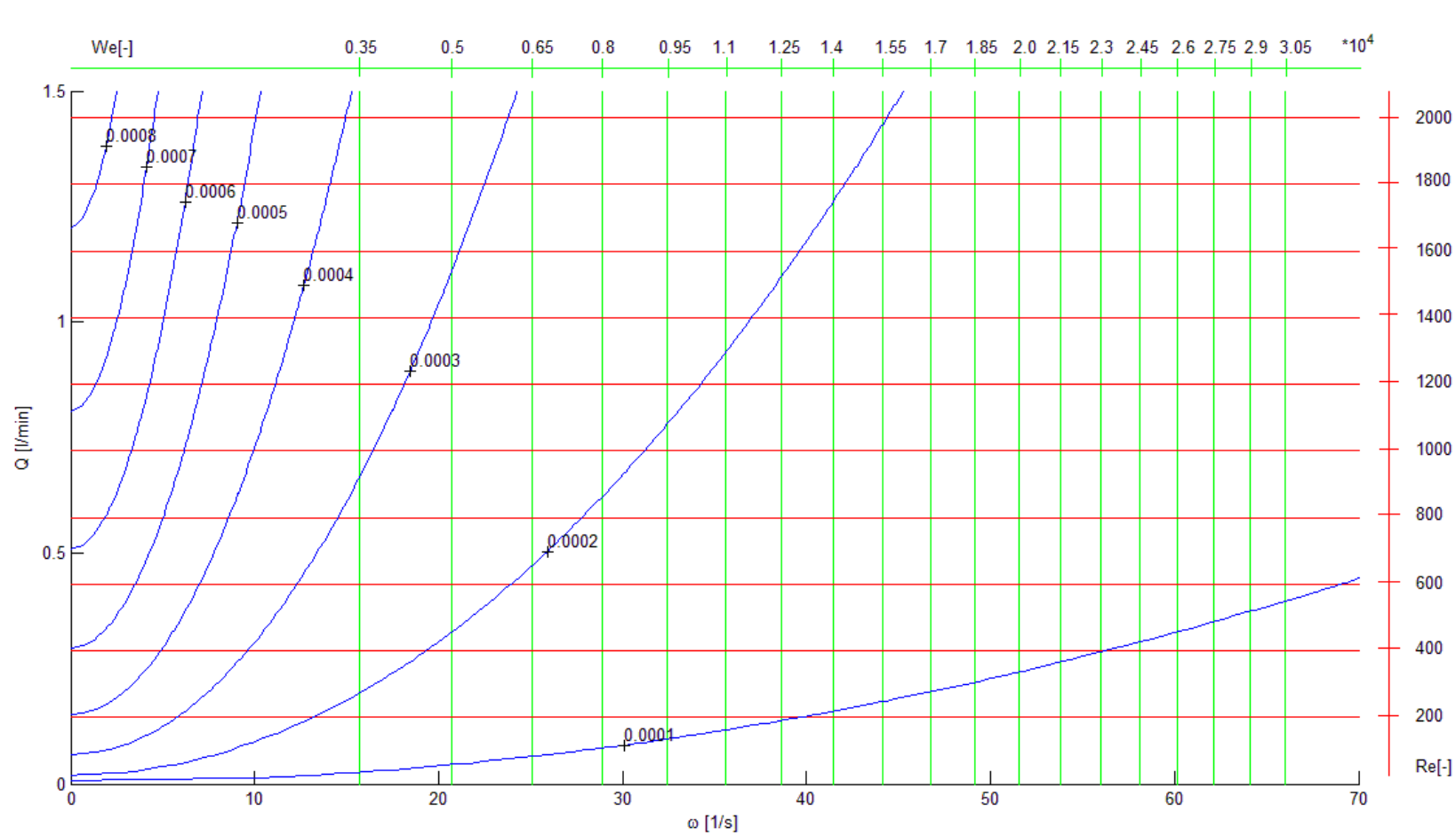


Figure 22: Characteristic of Delta, the Reynolds number and the Weber number as function of rotational speed and volume flow

2.3. Film improvement

To improve the film flow on the paddle a literature research has been done. The goal is to design a new canal shaped form that will lead to a laminar stable film flow on the paddle. In Fig. 20 the two geometries that already have been made are pictured. Both have already been tested in the research of V. Rohwedder [28]. They will be tested in more detail in this research. The actually testing will be done in the experimental sections: 2.4 and 2.5. With the shape the water flowing out of the flywheel will be led onto the clear part of the glass plate, hence the bottom part of Fig. 18. On this part of the glass plate the thin film will form. Also on this part the droplet impingement would take place in the droplet impingement experiment [7]. It is therefore important that the thin film on this place is smooth and laminar. There must be as little disturbance in the flow as possible. The droplet impingement on the paddle will however not be a part of this report. The research only focuses on the development of a smooth thin film.

Y. Su did a research on the rectangular contractions of three-dimensional wind tunnels [16]. Su states that there is no advantage of designing a wind tunnel contraction with cross-section similarity. Cross-section similarity is the worst possible geometry for wind tunnels with a narrow outlet. For wind tunnels a square inlet is a good choice no matter what the ratio of the rectangular outlet is like. Su takes these conclusions based on the height of the pressure coefficient and the non-uniformity of the velocity near the entrance and exit of the contraction. In the case of the thin film research the uniformity of the velocity is of great importance. However there should be noted that the research of Y. Su is for wind tunnels hence for compressible flow. Compared with the flow of a wind tunnel the flow of water is incompressible. Also the dimensions of a wind tunnel are much bigger than the dimensions of the canal shape in this report. Also an important footnote is that the conclusions of the form of the cross sections have been taken for a specific cubic contour [17] of the wind tunnel.

H. Fujimoto et. al. investigated the flow characteristics of a water jet impingement on a moving surface with a thin water film [18]. They also used a canal shaped geometry to produce a thin film on a surface, Fig. 23.

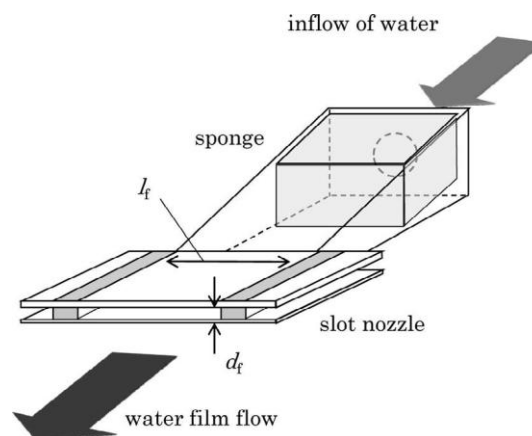


Figure 23: Nozzle shape to create water film [18].

The canal consists of two parts, a convergent part and a straight part. The convergent part that is used keeps always the same rectangular cross section ratio. The cross section decreases monotonically towards the outlet. In the uniform part two parallel plates are being used. The flow length of the uniform section can be changed. If the distance between the two plates is larger the

flow length becomes larger². Another interesting fact is that Fujiimoto et. al. use a sponge in the inlet of the convergent canal, Fig. 23. The sponge will minimize flow disturbances [18].

In the book Open-Channel Hydraulics [19] by Ven Te Chow another interesting fact was found. Chow makes a statement about transitions at pipe, flume and canal outlets. Chow states that the optimal angle of lateral convergence at contractions is given by an angle of 12.5°. This angle is the optimum maximum angle between the channel axis and the line connection the channel sides between entrance and exit sections [19]. Chow also states that sharp edges in the structure should be avoided because they will induce turbulence in the flow. A note here is that the dimensions of the channels are much greater than the dimensions used in the flywheel experiment.

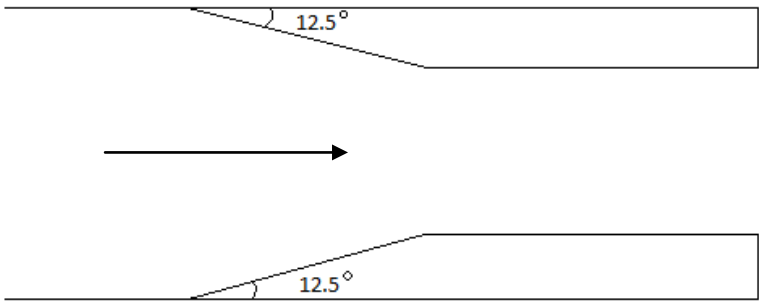


Figure 53: Optimal contraction angle by Chow [19].

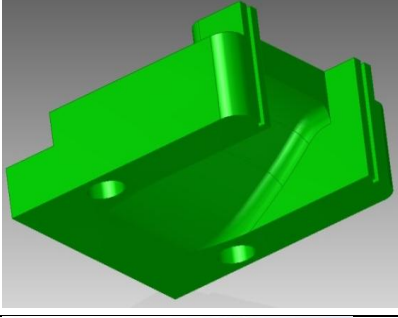
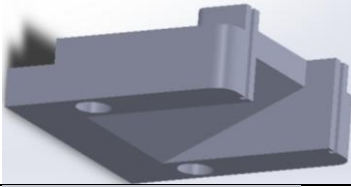
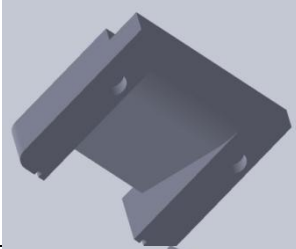
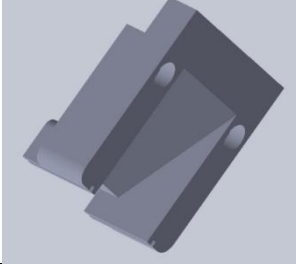
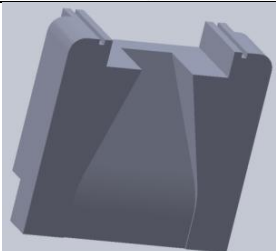
New Geometries

With the theory from the literature research, a few new designs for a canal have been made. The designs are variations on the design made by V. Rohwedder, Fig. 20. The dimensions of the total shape are for all the geometries the same. Only the canal shape inside the geometry is different every time. Every design has two holes in the bottom. These holes are necessary because of the screws which attach the metal plates onto the glass plate. Every geometry has two small vertically running slits at the back. In these slits a rubber *o-ring* string will be glued. This has been designed by V. Rohwedder to enhance the waterproof fitting in the Aluminum housing. In Fig. 25 this slit with a rubber wire in it can be seen. The left picture is the complete paddle with the Aluminum cover on it.

In Fig. 24 the new designs have been given, geometries 1, 2 and 3 are the designs that already have been made. The Solidworks® drawings for the newly designed geometries can be seen in Appendix A.

<p>Geometry 1</p> <ul style="list-style-type: none"> • Paddle design by Faßmann • Convergent roof 	
---	--

² For a distance $df=2\text{ mm}$ the length is 76 mm , for a distance $df=4\text{ mm}$ the length is 100 mm .

<p>Geometry 2</p> <ul style="list-style-type: none"> • Design by Rohwedder • Wind tunnel shape roof 	 <p>[20]</p>
<p>Geometry 3</p> <ul style="list-style-type: none"> • Design by Rohwedder • Same convergent roof as the paddle of Faßmann 	
<p>Geometry 4</p> <ul style="list-style-type: none"> • Variation on geometry 3 • Fillet R20 at outlet • Rim on the roof higher³ 	
<p>Geometry 5</p> <ul style="list-style-type: none"> • Variation on design 3 • Only difference: rim on roof higher 	
<p>Geometry 6</p> <ul style="list-style-type: none"> • Roof and walls are convergent • Roof has same angle as design 3 • Walls have angle of 12.5° [19] • Fillet R20 at outlet and walls • Pre-defined canal, use of metal plates is not needed 	
<p>Geometry 7</p> <ul style="list-style-type: none"> • Divergent canal • Square inlet area [16] • Fillet R20 at outlet • Uniform outlet part of height 0.3 mm, use of the metal plates is not needed 	

³ The rim on the roof of the shape should fit tight in the slit in the metal plate, Fig. 21. In geometry 2 and 3 this rim wasn't high enough to ensure a waterproof closure. In the rest of the designs this rim has been made higher. For details see Appendix A.

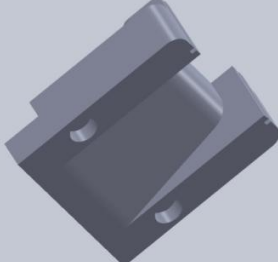
<p>Geometry 8</p> <ul style="list-style-type: none"> • Roof has convergent angle of 12.5° [19] • Inlet has fillet of R5 		
---	--	--

Figure 24: Designs of the canal shaped geometries

The new geometries have been made by the use of a 3D-printer at the ISM⁴. The advantage of a 3D printer is that it is a fast method to create the designs. Printing was done in about 3 hours, independent of the amount designs printed. The method is also way cheaper as the CNC-milling used before. Downside is the accuracy of the dimensions. The 3D printer uses a polymer for the printing with the same properties as polyethylen. The plastic is easily processable. With P2000 sandpaper the canal is smoothed after the printing. The cooling down process of the plastic made it a little bit bigger than it was designed. With the sandpaper it has been ensured that the canal shaped geometry fits tight in the Aluminum housing. Also the holes in the geometry had to be made a little bigger. In Fig. 26 a printed geometry can be seen, geometry 7. This geometry has been given a slit height of 0.3 mm to account for the inaccuracy of the 3D printer.

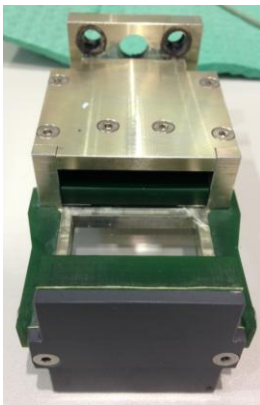


Figure 25: Left: Complete paddle with cover on it, Right: Geometry 3 with the rubber wire in the slit.



Figure 26: Geometry 6 printed with the 3D printer

⁴ Institut für Strömungsmechanik

2.4. Flywheel experiment part A

The goal of this first experiment is the ranking of the designed geometries. This experiment will be completely static, meaning that the flywheel, at which the paddle with the designed geometries will be attached, will not spin. Goal is to compare the newly designed geometries with the two old ones and with the old paddle from Faßmann. The two old geometries and the old paddle will thus also be tested. Observations in the film flow will, for yet, be made with the naked eye. Pictures will be taken with an 8 megapixel camera. A ranking will be made in the geometries, the one with the best overall result will also be tested in experiment B (section 2.5).

2.4.1. Set-up

Structure

The experimental set-up for this first experiment is based on the set-up of Faßmann and V. Rohwedder. The set-up of Faßmann is pictured in Fig. 15. In the set-up for the experiment of this report, the actual droplet impingement will not be done. Only the film flow on the paddle is important in this research. For the experiment the flywheel designed by Faßmann [7] will be used. This flywheel is attached to a steel stand which is attached to the concrete floor. The flywheel is attached to the stand by means of a fixed-loose bearing⁵. In Fig. 27 one side of the flywheel has been pictured. At this side also the connection to the motor and the light-cabinet can be seen. Both of them have, for yet, no use. In experiment B this will be further explained. At the lateral side of the flywheel the paddle will be attached.

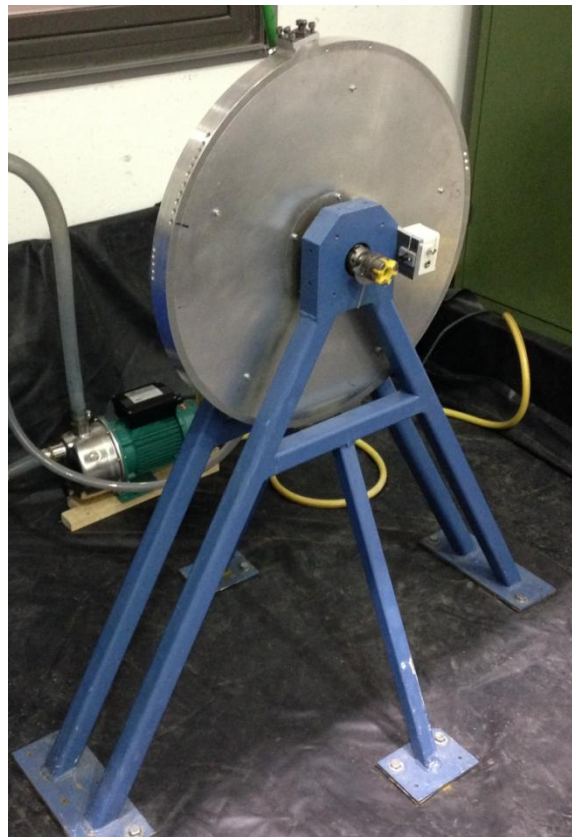


Figure 27: Flywheel attached to the concrete floor

⁵ FLL: Fest-Los-Lagerung

There are two different paddles, the old one from Faßmann (Fig. 16) and the new one from V. Rohwedder (Fig. 17). The new paddle must be attached in a different way than the old paddle. The old paddle from Faßmann can be direct attached to the flywheel with the help of two M6- and two M3-screws made out of Titanium. The new paddle that will be used in this report is attached to the flywheel with the use of another piece made out of Aluminum, a flange plate. This connection can be seen in Fig. 28.

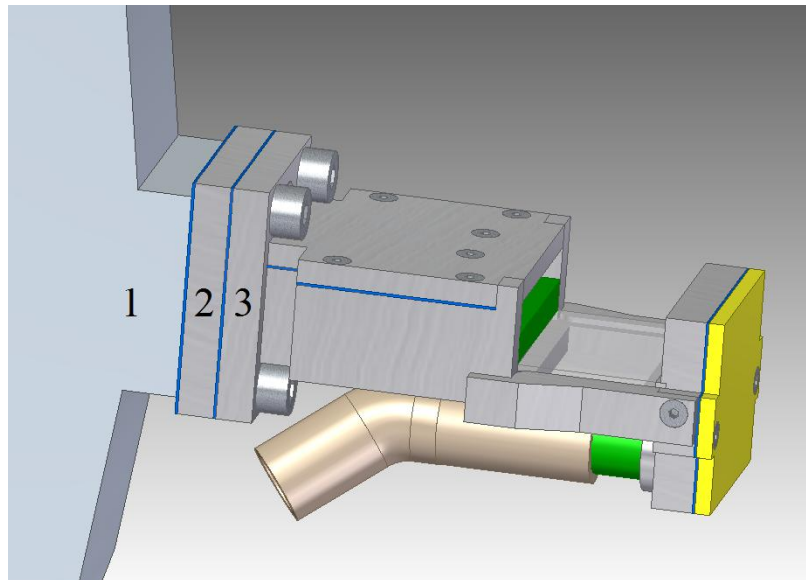


Figure 28: paddle connected to the flywheel: 1) flywheel 2) connection plate 3) paddle [21]

The paddle will be screwed with four M6-screws to the middle plate. These screws have been made out of Titanium to prevent corrosion and because of the weight. The middle plate is attached to the flywheel with the original M6- and M3-screws. The function of the flange plate is to ensure a safe strong connection of the paddle to the flywheel. The helicoils in the flywheel have been worn out over time. With the flange plate, V. Rohwedder tried to solve this problem. The strong connection is also another reason why the screws have been made out of Titanium. This is needed because of the high rotational velocity of the flywheel, hence the high centrifugal force. At the other side of the flywheel a counterweight has been attached. The counterweight and the attached paddle can be seen in Fig. 29. This counterweight has been attached to balance out the paddle.

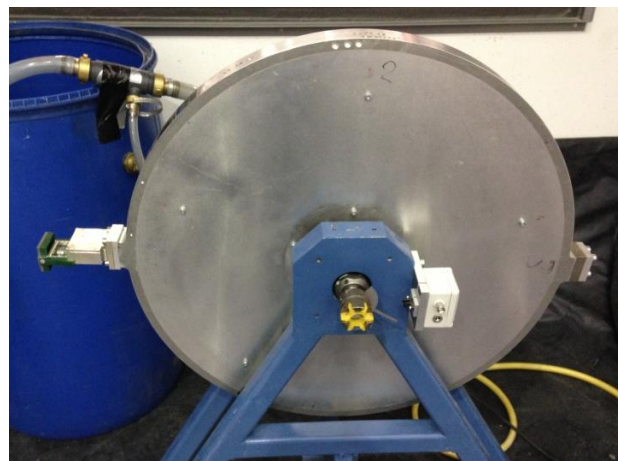


Figure 29: Paddle attached to flywheel and counterweight

Watercycle

In Fig. 30 the water cycle of the flywheel experiment can be seen. The main cycle consists out of a water barrel partly filled with water. The water tank forms together with a pump a cycle. This cycle is connected to the flywheel through a water jet pump. The flywheel is connected to the water connection from the ISM. Between the flywheel and the connection from the ISM a volume flow meter is situated. The type of the pump, flow rate meter and water jet pump has been given in appendix B.

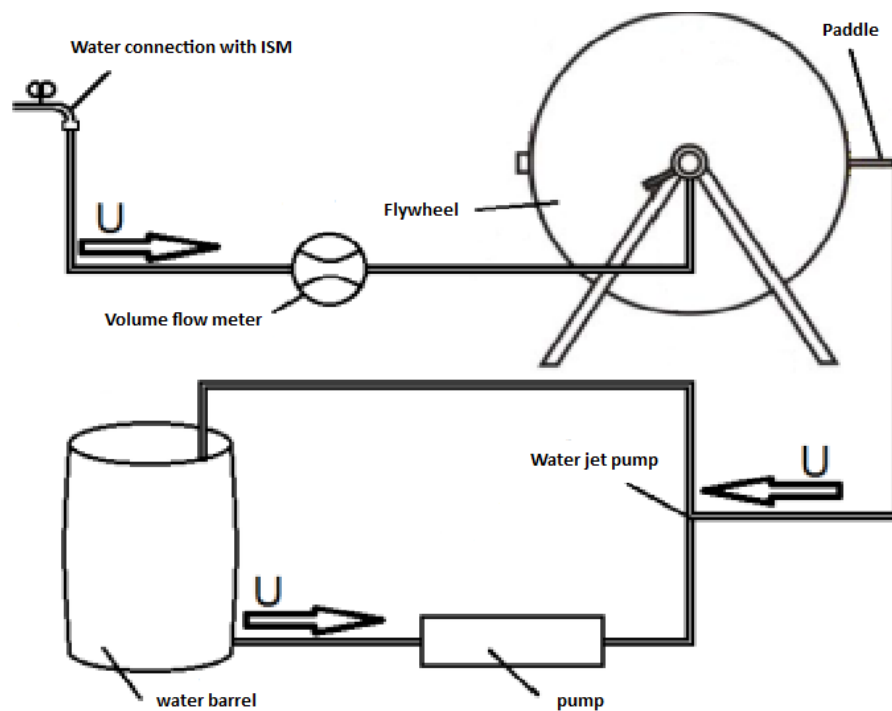


Figure 30: Water cycle flywheel experiment [7] [22]

The outlet from the paddle is through a silicone-textile hose connected to the flywheel. This hose has flexible qualities and has also good buckle qualities [28]. The buckling of the hose depends also on the connection with the paddle. The flywheel is then connected with a normal PVC hose to the water jet pump. The water jet pump is based on the Venturi effect. A reduction in the cross section creates a reduction in fluid pressure. This provides the sucking power that will ensure the extraction of the water flow from the paddle. A picture of the experimental set-up with the water cycle has been given in Fig. 31.

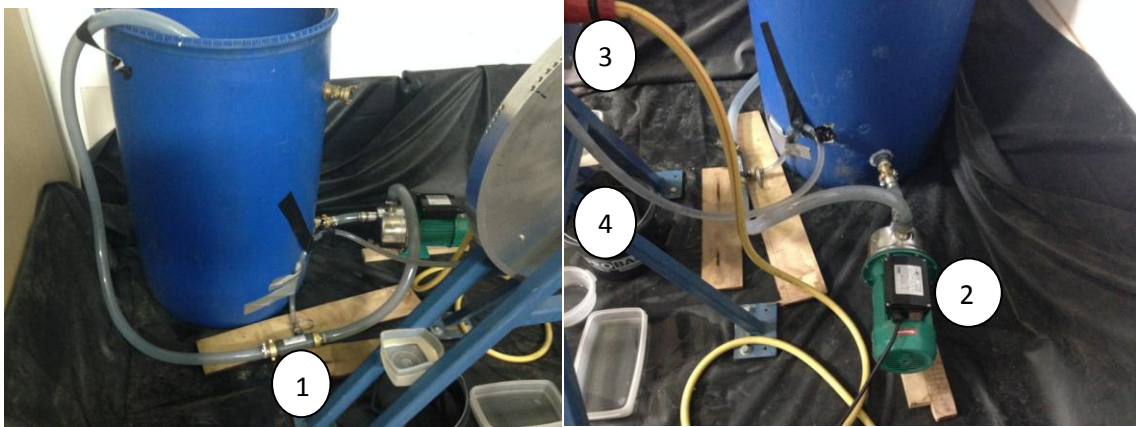


Figure 31: Water cycle flywheel experiment. 1) water jet pump 2) pump 3) connection flywheel to water connection of ISM 4) connection flywheel to water jet pump

Waterproof

For the film flow on the glass plate it is very important that the flow from the flywheel onto the glass plate is waterproof. To ensure the sealing of the paddle a few measures were taken.

- Between some pieces a high pressure sealing paper was used. This paper, Centellen® WS 3820, was also used in the research of V. Rohwedder [28]. In [fig. 28](#) the places where this paper was used can be seen, the paper has been given a blue color. In [Fig. 17](#) and [Fig. 18](#) the places on the paddle where this paper has been used can be seen. The paper was attached on both the edges.
- The u-shape on top of the paddle also creates a sealing, [Fig. 32](#). On top of the view from [Fig. 32](#), the cover is placed, with a u-shape slit in it. Between the canal shaped geometry and the cover steel leaf springs have been placed. This ensures that the geometry is tightened onto the plates. The cover is attached to the geometry through screws.

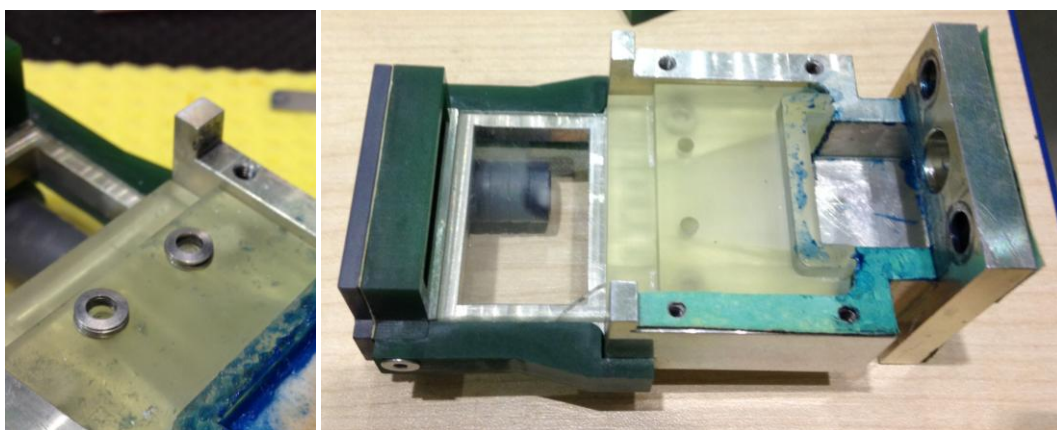


Figure 32: Left: leaf springs, right: u-shape and sealing paper

- To improve the sealing of the paddle and the sealing of the paddle to the flywheel also a paste has been used. The long duration paste Hylomar® M has a mechanical and thermal resistance against water [28]. The paste has been used on the paper and on the u-shape on the geometry (the blue substance in [Fig. 32](#)). The connection point between the paddle and the flywheel was

also lubricated with the paste. The use of too much paste however has a negative effect. The paper will swell and eventually will tear.

- On the heads of the two M6- and two M3-screws that connect the middle piece to the flywheel, seal tape has been used to prevent water coming through the screws.

2.4.2. Results

All the 7 geometries and the old paddle from Faßmann (geometry 1) have been tested on the thin film flow that leaves the geometry. Only the smaller plates have been tested, the left ones in [Fig. 19](#). Hence a slit width of 24 mm has been applied. The new geometries have been designed to be applied to the smaller plates. Because the research of V. Rohwedder was only done for a slit height of 0.1 and 0.3 mm [28], a slit height of 0.2 mm has been tested for. This was realized by placing two 0.1 mm plates on each other. The plates had been fabricated before for usage in the earlier research. Again it should be noted that this section for now only focuses on the static film flow on the paddle without any rotational influences of the flywheel. Goal is to select the best geometry which then will be tested with the rotation of the flywheel, in section 2.5. The next tests have been done on the geometries:

- The horizontal position of the paddle. The flow rate have been increased starting with the minimal flow rate, the flow rate at which just a thin film appeared. Pictures have been taken at two increased flow rates and at the highest flow rate. This was the flow rate at which the film became fully turbulent. The two flow rates in the middle have been taken approximately the same for every geometry.
- The same has been done for two higher angles, 20° and 45°, with the direction upwards.
- Pictures have been taken for higher angles at one flow rate, for every geometry approximately 0.9 l/min, starting at horizontal position moving to vertical position upwards.
- The theory from [18], section 2.3, has also been tested. That is the minimization of flow disturbances by putting a sponge in the inlet of the canal. Four filters have been tested, see [Fig. 33](#). The filters have been made out of different types of Polyethylen. The filters have been cut to the right size with a cutter and are placed in the inlet of the geometry. In [Fig. 33](#) two examples have been given. A few geometries have been tested with these filters. The best filter has been selected. The first two points from above have been tested with the filters.

	Filter 1	Filter 2	Filter 3	Filter 5
Polyethylen	UHMW-Polyethylen	UHMW-Polyethylen	HD-Polyethylen	UHMW-Polyethylen
pore diameter	20 μm	35 μm	150 μm	250 μm
dept	6 mm	10 mm	3 mm	5 mm

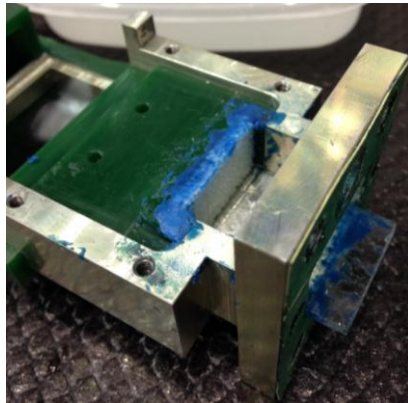


Figure 33: Above: the 4 filter, Left: filter 3 applied to geometry 2, right: filter 2 applied to geometry 7

The geometries have been rated based on the next subjects:

- The overall smoothness of the film. How many disturbances were observed in the middle of the film?
- What was the shape of the film? Was the shape more like a small triangle or a like a wide rectangle? For the stability of the film at higher rotation the shape will be important. Also the shape is important for the situation that the flywheel rotates. The rotation changes the shape of the film.
- The amount and the height of waves in the film and at the side of the film. The amount of waves in the film is correspondingly to the smoothness in the film. The only difference is that sometimes there were waves observed in the film caused by other influences than the shape of the canal. This was different than the disturbance observed in the film caused by the shape of the canal, the smoothness of the film. The waves at the side were caused by the shape of the canal and mostly by the steel plates under the designed geometry shape. These waves were sometimes so high that they had influence on the smoothness of the film. High waves are thus unwanted.
- How did all of the above points changed when the flow rate and the angle of the paddle was changed.

The results of the observations of the film on the paddle can be seen in [Fig. 34](#).

Geometry	Waves in film	Waves on edges film	Width film	Stability at higher angle	Stability at higher flow rate	Smoothness film
1	0	--	++	0	-	-
2	--	--	--	0	--	--
3	+	--	--	-	+	++
4	++	+	+	0	++	++
5	+	+	-	0	--	+
6	+	--	--	-	0	+
7	++	--	-	--	-	++
8	+	-	+	--	--	+
worst -- - 0 + ++ best						

Figure 34: Table with results of the experiment observations

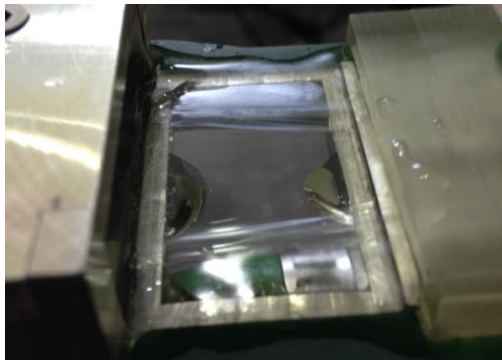
From these results, geometry 4 has the best results. In Fig. 35 some results of this geometry have been given. Compared with the other geometries, geometry 4 stands out by “the waves on the edges of the film” and “the width of the film”. Also the performance at higher angle and higher flow rate is better compared to the other geometries. In Fig. 36 those points of geometry 4 have been compared with the worst geometry for each point. Some important observations have been given below, the pictures of the examples are given in Fig. 36:

- For geometry 4 there were wave Mountains on the edge of the film. Those were there on every film, from every geometry. In the worst case, for example geometry 7, there were many waves which also had an influence on the thin film. The waves seem to decrease in height towards the middle of the film, giving the film a triangular shape. In the best case, geometry 4, the waves have very little influence on the smooth middle part of the film. The cause of the waves seems to be the edges of the uniform part of the canal. Especially the geometries with the pre-defined canal, without the use of the metal plates, have much waves at the side. The reason for this is the finishing of the underside and the edges of these canals. The use of the metal plates gives a better result. At a higher flow rate there will however be an additional flow through the slit between the plates and the glass plate. This will create the wave mountains at the edges of the film.
- The width of the film seems to be purely an effect of the shape of the canal. For every geometry it is stated that with an increase of the flow rate the film starts as a small triangle and turns into a strip. With the best geometry the strip will be wide and with the worse geometry the strip never forms. The small triangular form of the film can be explained with the theory. In section 2.2.1 is explained that the velocity profile has a velocity of zero at the wall, the no-slip condition. This is the reason why the velocity in the middle of the film is higher than at the edges. Hence when the flow rate is low a triangular shaped film will form.
- The stability at higher angle is very dependent of the backflow of the film. With a high flow rate the film bounces of the back of the outlet on the film. This causes a disturbance of the film in terms of smoothness. With all the geometries the minimal flow rate increases with the increase of the angle. If the angle goes up, the flow turns into a triangular shape. This shape turns more

into a strip if the flow rate goes up but this causes more disturbances because of the backflow. This happens with every geometry and the differences between them are small on this point.

- Two important factors that influence the stability of the film at high flow rate are the backflow and the turbulence. For geometry 4 the film at high flow rate is still quite wide and smooth in the middle. For geometry 8 the film has many disturbances, a lot of waves occur in the film. This can mean that the film has become turbulent or that the influence of the backflow, which occurred, became too strong.

Waves on edges of film

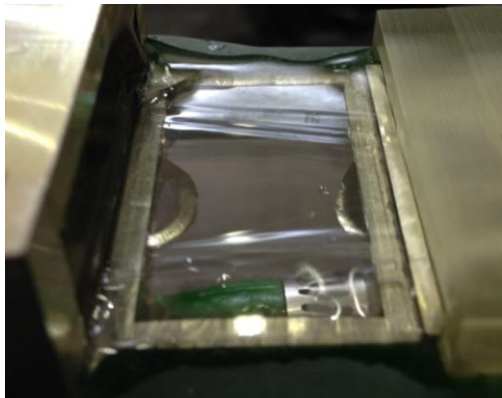


Geometry 4, 0°, 1.05 l/min

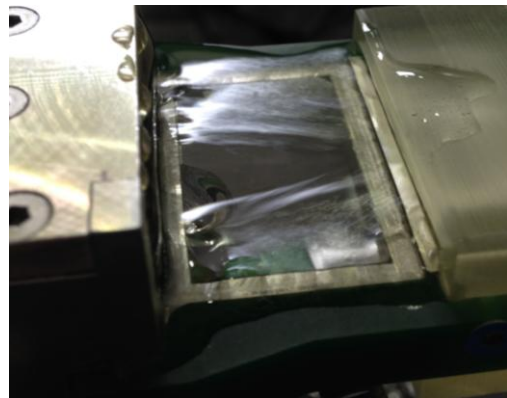


Geometry 7, 0°, 1.10 l/min

Width of film

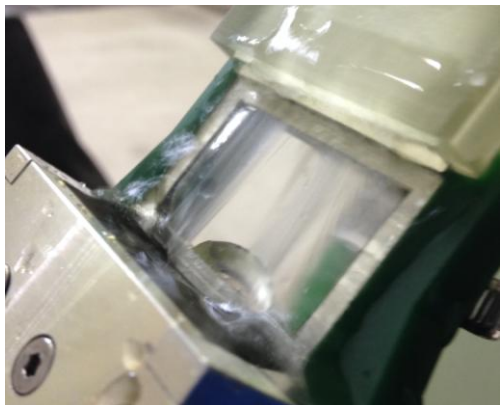


Geometry 4, 0°, 0.84 l/min

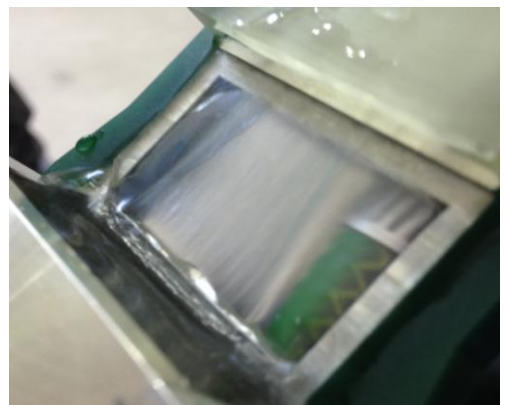


Geometry 5, 0°, 0.79 l/min

Stability at higher angle

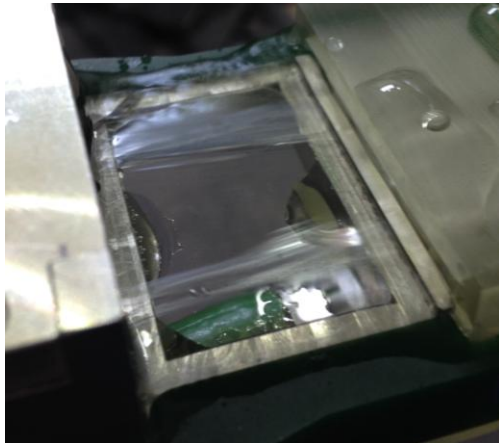


Geometry 4, 45°, 1.33 l/min

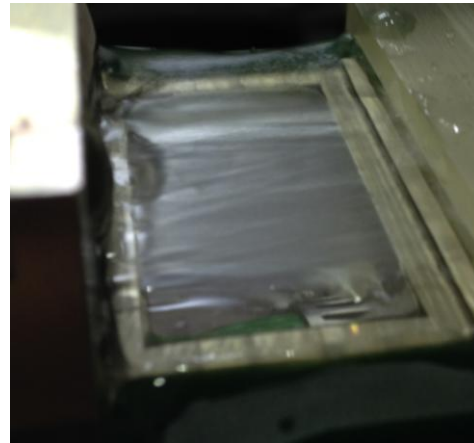


Geometry 7, 45°, 1.33 l/min

Stability at higher flow rate



Geometry 4, 0°, 1.35 l/min



Geometry 8, 0°, 1.39 l/min

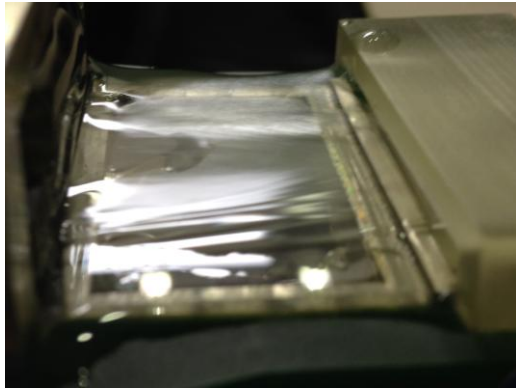
Figure 36: Comparison between geometry 4 and worse geometries

Filters

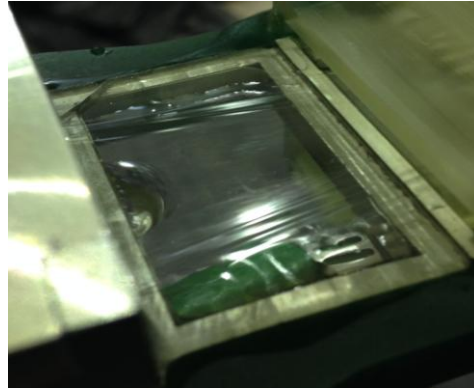
The influence of the filters, [Fig. 33](#), has also been tested. First the best filter has been chosen. Observed was that if the pores of the filter were too small, the pressure in the canal became too high. This caused a lot of leakage that couldn't be stopped by the adding of extra paste between the slits or by applying tape on the screws. If the pore diameter became too high the filter didn't have any influence on the film anymore. Therefore after applying all the four filters to a geometry, geometry 2, filter 2 has been chosen as the best filter. In general the applying of the filter caused the flow to decelerate, which causes less disturbance in the flow and less backflow. The applying of a filter is in that way a bit fooling because it seems to be that the filter just decelerates the flow. However there were some exceptions, see [Fig. 37](#). Here the applying of the filter causes a flow with fewer disturbances. It can also be seen that the flow in these cases doesn't really seem to decelerate because the shape of the flow doesn't adopt the typical triangular shape.

2.4.3. Discussion

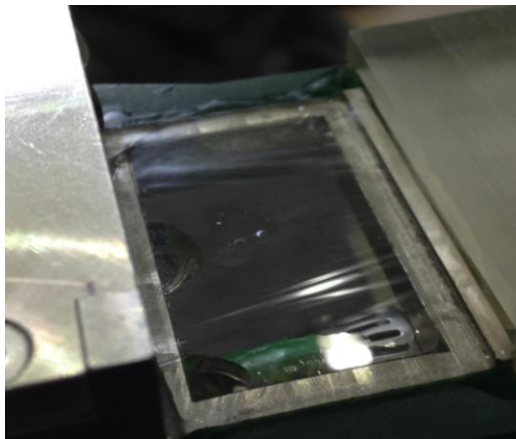
The results showed that geometry 4 was the best geometry for the static case. This geometry will thus be tested in the second experiment with the rotating flywheel. Geometry 4 stood out above the rest by a few factors. The film was smoother compared to the rest, less waves were observed. Also was the film smoother at a higher flow rate. Since the rotating flywheel experiment will be done with higher flow rates, this is an important factor. There are however a few butts with the choice of this geometry. Also there were a few problems during the experiment that slowed down the process. During the experiment a few adjustments were made from which some had a positive result.



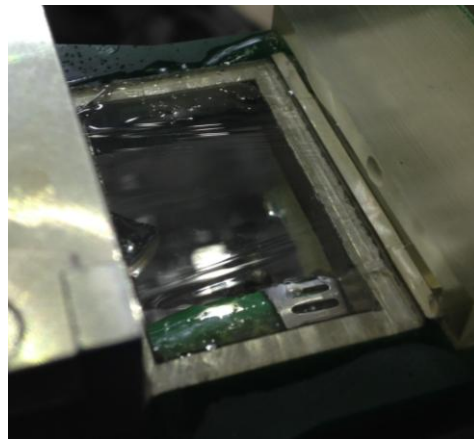
Geometry 8, 0°, 0.94 l/min



Geometry 8 with filter 2, 0°, 1.01 l/min



Geometry 4, 0°, 1.05 l/min



Geometry 4 with filter 2, 0°, 1.04 l/min

Figure 37: Geometries with filter 2 with a better result

Leakage

The leakage of water between different slits of the paddle was a big problem. Different kinds of leakage were observed during the experiment, some had influence on the film flow. Those can be seen in Fig. 38. Especially when the pressure in the canal became too high, by applying a too dense filter, there was leakage detected from above the 0.2 mm outlet slit. This was partly solved by applying more sealing paste on the u-shape of the canal shape, Fig. 33 left picture. But for the dense filters this problem kept existing. The other kind of leakage had influence on the visibility of the film. The quartz glass plate that was used had been used in the flywheel experiment before. There was a fracture in the glass plate and because of that water could run under the glass plate. There was tried to minimize this by tightening the geometry on the glass plate, but this couldn't be too tight because then new fractures would occur.

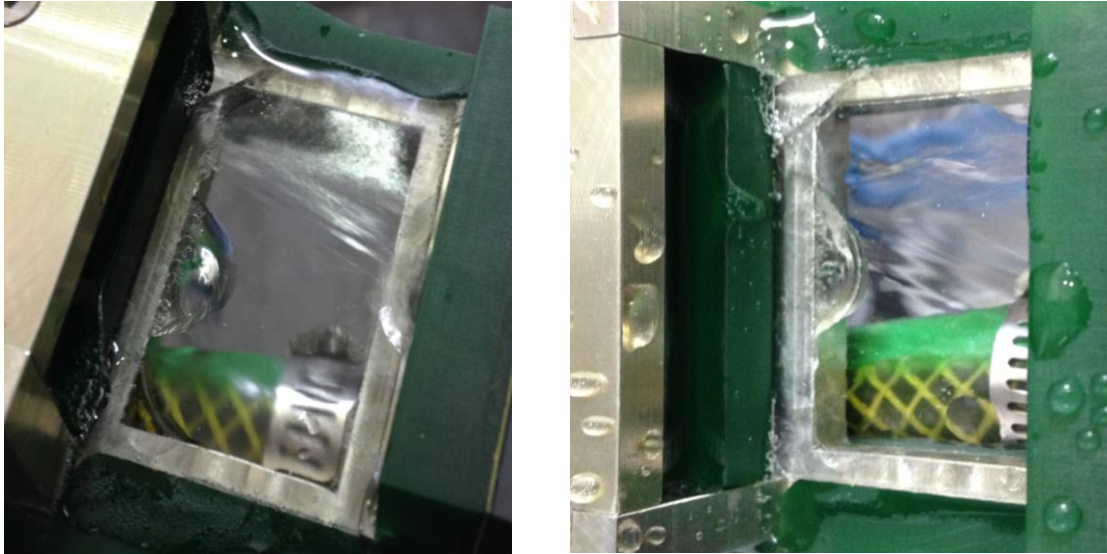


Figure 38: Left: leakage under the glass plate, Right: leakage from above the outlet of the canal

Also another form of leakage was observed; leakage between the holes of the screws and leakage between the connection of the paddle to the flywheel. The solving of this leakage problem by tightening the paddle to the flywheel caused another problem: Damage to the screws and the sealing paper, see Fig. 39. The damage of the sealing paper was also caused by the use of too much paste and too small holes for the screws. New stainless steel screws were applied and new sealing paper was used. The leakage problem between the holes of the screws was solved by using sealing tape on the heads of the screws. Paste was carefully applied around the holes of the screws and around the canal. This eventually solved the problem.

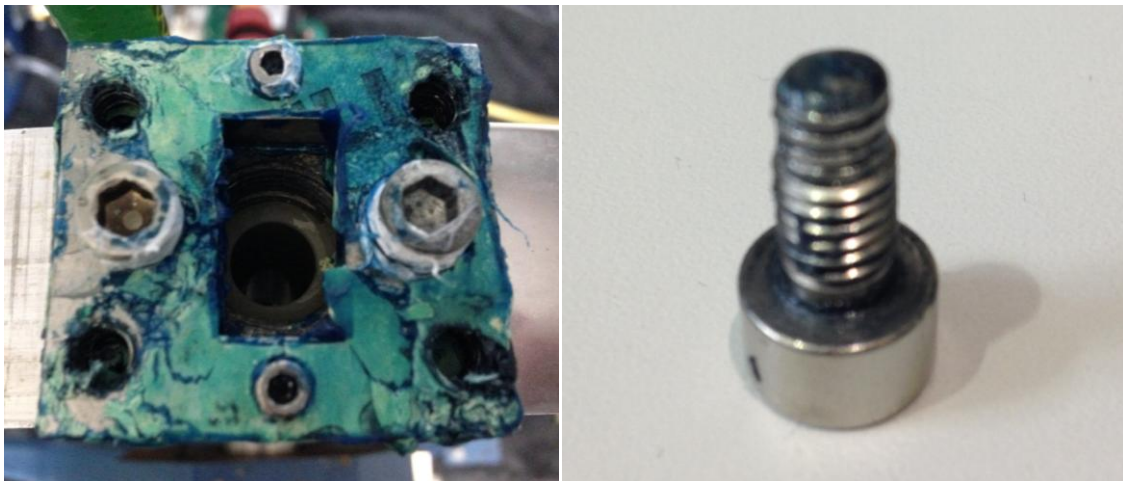


Figure 39: Left: Damage of the Centellen® WS 3820 sealing paper, Right: damage of the thread of the 4 Titanium M6 screws.

A great part of the leakage in general was caused by the precision of the 3D-printer. After the printing a lot of sanding has been done on the geometries by hand because of the bad accuracy of the 3D printer. This sanding by hand doesn't assure a straight finish of the bottom and the angles of the geometry. To have a better finish another producing method is advised: CNC milling, which also has been used to produce the geometries 2 and 3. Through time and money issues the 3D printer has

been used for now. The amount of designs made it more logic to use the 3D printer at first. To produce that much design with milling would be very costly.

Backflow

Another problem that occurred was the backflow of water onto the thin film. Especially the high angles and the high flow rates caused the water to bounce back onto the thin film. This caused disturbances in the flow. A solution has been found by changing the outlet of the paddle. The new outlet has been designed by V. Rohwedder during the internship. The new outlet can be seen in Fig. 40. The new outlet has been made lower. The slit in which the water film flows has a lower ceiling. With this lower ceiling less air flows in the outlet together with the water. The air in the water causes bubbles and thus turbulence in the stream. Also the backside of the outlet has been made longer to remove the bulging current. In the outlet a shape has been placed made of clay paste, Fig. 40. This shape makes the flow more streamlined and decreases the bouncing of the water on the backside, the case, of the outlet.

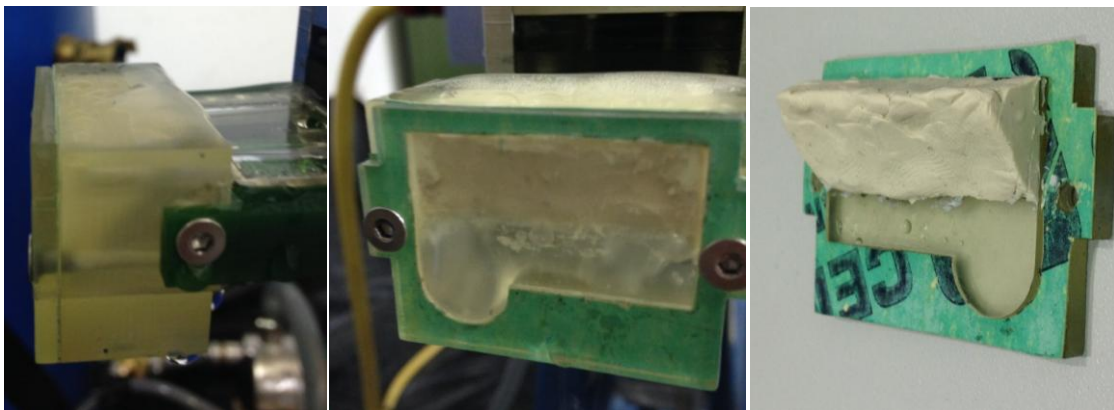


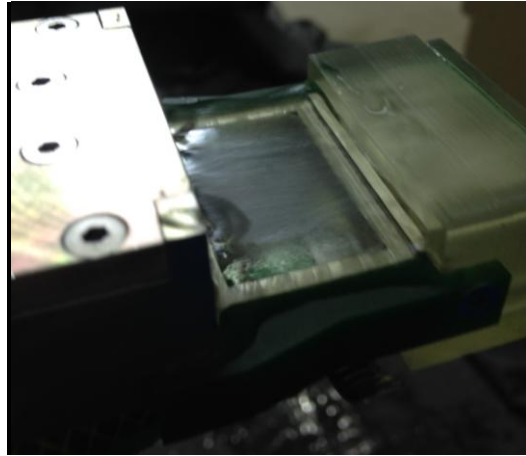
Figure 40: Left/middle: new outlet geometry, Right: case of the outlet with clay shape

The new outlet also has been made with the 3D printer. Thread for the attachment to the paddle was made after the printing. Sealing paper has been used on the case of the outlet to prevent leakage. In Fig. 41 the two different outlets have been compared with each other. Geometry 3 and geometry 5 have been compared with each other. Those geometries have the same canal shape with the only difference that the u-shape rim on top of geometry 5 is higher. In Fig. 41 can be seen that the paddle with the new outlet has much less backflow than the paddle with the old outlet. The new outlet has been tested on geometries 7, 8, 4 and thus 5. All these geometries gave a flow with little backflow. A good comparison only can be made between geometry 3 and 5 because they have the same canal shape. The result of the new geometry is thus only based on the comparison between these two geometries, in which the geometry with the new outlet had the lower amount of backflow.

A remark here is thus that the outlets haven't been tested with the same geometry due to time issues. This is a recommendation for a next experiment.



Geometry 3, 0°, 1.26 l/min



Geometry 5, 0°, 1.23 l/min

Figure 41: Left: old outlet, Right: new outlet

Position pump

The position of the water jet pump has also been changed during the experiment. For pictures of the water cycle see also Fig. 30 and Fig. 31. Three different positions have been tested for the water jet pump, see Fig. 42 for the two utmost conditions. In the left picture the water jet pump was placed at a high position, in the right picture on the ground. In the third position the water jet pump was placed at the same height as the paddle. At the high position the water jet pump wasn't able to suck all the water from the paddle up. The best position seemed to be the position where the water jet pump and the paddle were on the same level. This can be explained with a simple example. When two water basins are connected the pump needs less energy when the water in the two basins is on the same level.



Figure 42: Left: old position, Right: new position

Other

Another issue was debris in the water. This dirt was taken by the flow and became trapped in the slit of the canal. Then it caused disturbance of the flow. The dirt caused thin lines in the flow. The origin of this debris is not known, it could be caused by the water flowing from the connection with the ISM or the inside from the hoses. Further research of this debris under the microscope is advised. The problem was solved by cleaning the glass plate with Isopropanol and removing the dirt from the geometry or glass plate. This was however time consuming.

Another factor that caused insecurity in the results was the connection of the paddle to the flywheel. The outlet of the flywheel is round and the inlet of the paddle is rectangular, see Fig. 43. The passage is thus not smooth. In section 2.3 there has been found theory, Chow [19], which claims that sharp edges in passages should be avoided because they induce turbulence in the flow. It is however hard to make this passage smooth because then the whole paddle should be re-designed. After the connection between the paddle and the flywheel comes however a box shaped room which forms the inlet of the paddle. This room will function as a calming chamber and will take the turbulence for a big part out of the stream.

All these different influences made it hard to tell the difference between the different films on the paddle. The disturbance of the film was generally caused by the leakage that turned up at the higher angles and higher flow rates. This happened before the time that the film could actually turn fully turbulent. Another remark is that all the observations were made with the eye, no measuring device has been used.

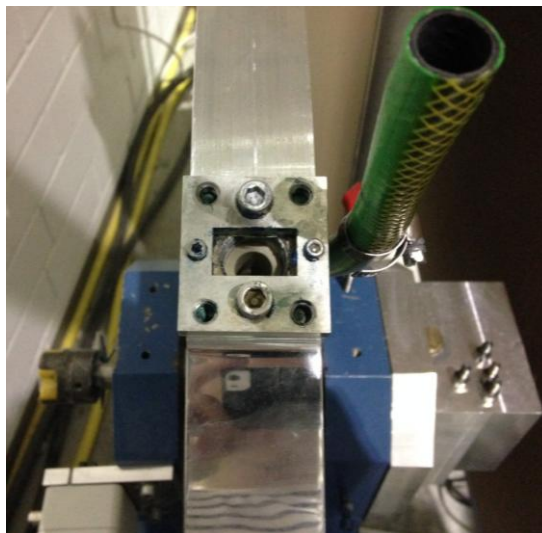


Figure 43: Passage from flywheel to paddle

2.5. Flywheel experiment part B

In experiment part A the best geometry for the static situation has been determined, geometry 4. In this section the geometry will be tested for a rotating flywheel. Goal is here to reach a Weber number of 10000. The experiment will have a completely different set-up as experiment A. Because of the high rotational velocity of the flywheel, safety has top priority in this experiment. A different measuring method has been used, the rotation of the flywheel makes it not possible to use the standard camera for pictures. In experiment B shadowgraphy has been used. Shadowgraphy is an optical method to observe flow variations in water and is suited to display the fluctuations in the film flow. A simple explanation has been given in Fig. 44.

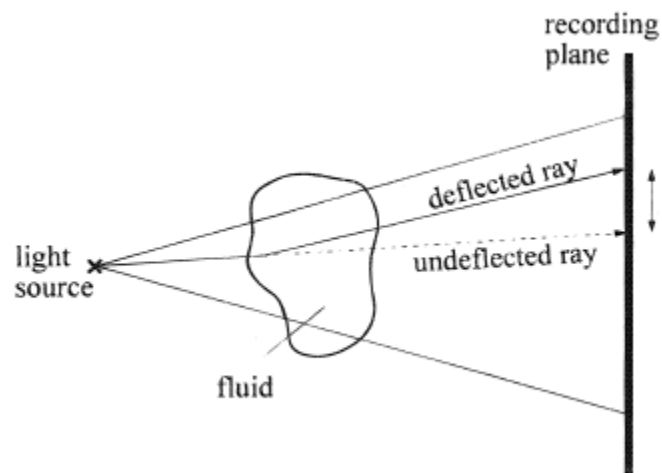


Figure 44: simple example of shadowgraphy [23]

The set-up for the shadowgraphy needs a light source (laser) and a recording plane (camera). The shadow of the varying density field of the fluid will be projected onto the recording plane. The position where the deflected ray ends on the recording plane is brighter than the undisturbed area. The position on the recording plane where the undeflected ray would end remains dark. For all the rays this will give a contrast on the recording plane [23].

Goals

The function of experiment B is to test the film quality of the paddle with geometry 4. The main goal of this testing is to get a laminar smooth flow with little fluctuations and backflow. The target is to reach this at a rotational velocity of the flywheel which gives a Weber number of 10000. The film shouldn't rupture and should stay attached to the glass plate. Also the flow rate should go beyond the value it had in experiment A, till around 2.0 l/min . In section 2.1 already has been pointed out that the geometry designed by Rohwedder, geometry 2 in this report, showed flow separation at Weber numbers of 5826 and 5106 for respectively 0.1 mm and 0.3 mm . At these points also the flow showed signs of turbulence. In this section a slit height of 0.2 mm has been tested for geometry 4. The main goal is thus to get a better result with this geometry than V. Rohwedder.

2.5.1. Set-up

Structure

To start the new experiment, the complete set-up from experiment A had to be rebuilt. This is because the wind tunnel area, where the set-up stood, was under construction. The set-up was rebuilt in a new room at the ISM. The set-up that has been used is based on the set-up used for the research of V. Rohwedder [28]. The water cycle being used is the same as in experiment A, see Fig. 30. The electrical set-up didn't change with the set-up used by Rohwedder, the mechanical set-up of the flywheel did. Both are being discussed below.

The mechanical set-up of the flywheel can be seen in Fig. 45. The flywheel is as before attached to the concrete floor screws. The motor (for the type see Appendix B) has been attached to the flywheel and mounted on X95 profiles. Important here is the diagonal carrier, which will be discussed later.

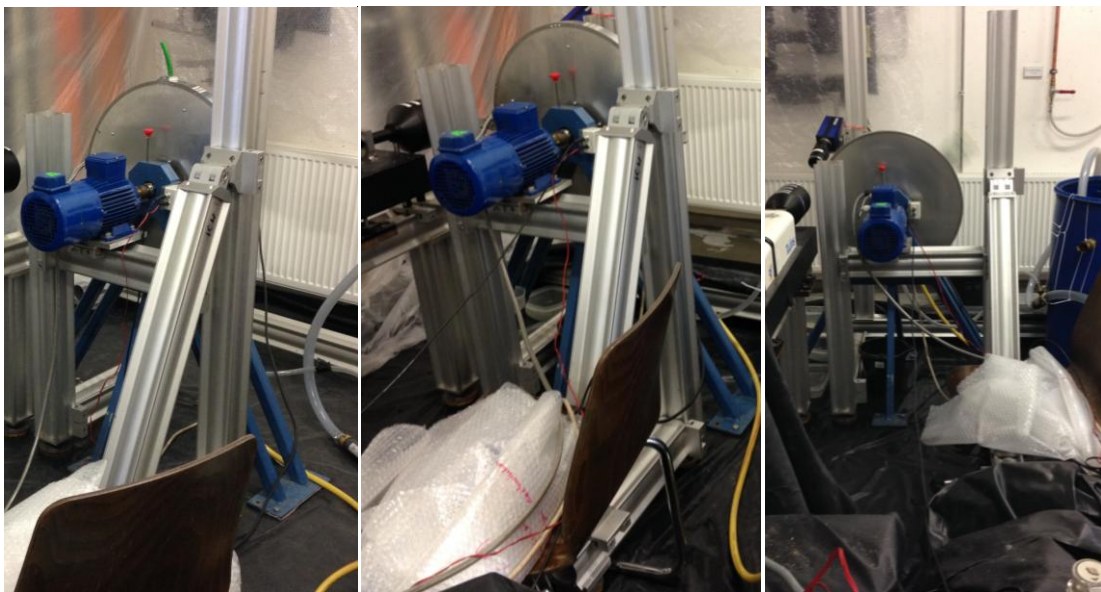


Figure 45: Attachment of motor to flywheel

The electrical scheme of the set-up can be seen in Fig. 46. The light source for the shadowgraphy is a laser of the type Nd: YAG Laser. This laser is operated by the PTU, the Programmable Timing Unit.

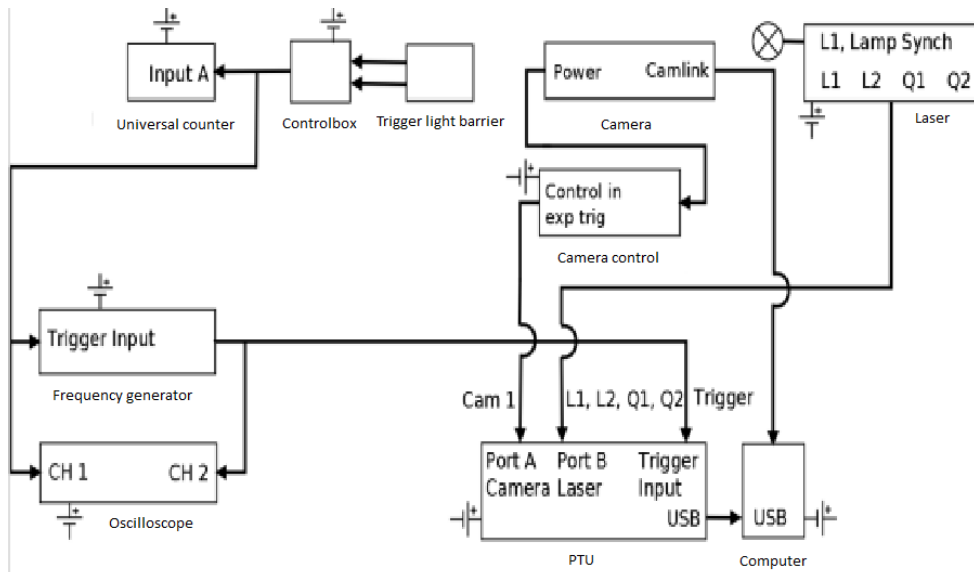


Figure 46: Electrical scheme of the experimental set-up [24]

At the blue frame which holds the flywheel a white box is attached, in Fig. 46 *Trigger light barrier*. At the axis of the flywheel a metal plate has been attached. The box and the plate can be seen in Fig. 29. At the moment that the paddle is at the horizontal position the metal plate crosses the light box. The box gives an impulse to the Universal counter, which indicates the exact frequency of rotation of the flywheel, and the *frequency generator*. The *oscilloscope* views the signal on a screen. The frequency generator enlarges the signal from the light box and gives this to the PTU. The PTU triggers the camera and the laser. All the details of the devices have been given in Appendix B. The set-up can be seen in Fig. 47.



Figure 47: Set-up of Experiment B

Safety

Because of the high velocity of the flywheel certain safety precautions had to be taken:

- The electrical devices were covered with plastic sheets. Also the floor was covered with a plastic sheet for the water leakage from the paddle. Some parts of the walls have also been covered with sheets. The plastic on the floor created a kind of pool. This was needed because of the high risk of water spilling on the floor because of the amount of water involved in the experiment. During the internship a hose fell out of the water barrel in the weekend because of bad attachment. This caused the floor of the room to flow full of water. However the plastic pool prevented worse. After this accident the water hose was attached to the barrel with tie wraps and the pool was improved by making the edges higher.
- Cables were taped on the floor. This prevented tripping over the cables by people. Also it was an organizing method.
- The motor has been fixed extra with a diagonal X95 profile, Fig. 45. This is actually not a security method. The extra profile will provide more stability to the flywheel. When the speed of rotation of the motor is not constant this can cause the flywheel to shake and thus the film to become unstable.
- During the experiment the operators were not allowed to stand in the line of the rotation of the flywheel in case some parts of the flywheel let go.
- The laser was equipped with a diffuser. Diffusers increase the size of the laser beam hence decrease the strength of it. Nonetheless people weren't allowed to stand in the laser during the experiment.

2.5.2. Results

First a static experiment was done to find the right camera settings and the right position of the camera, see Fig. 48. The camera couldn't be in the path of the laser because this led to a bad lighting. Also the camera couldn't stand too close because of the splashing of water. The main control of the laser and the recording of the pictures have been done with the program DaVis 7.2 ParticleMaster.

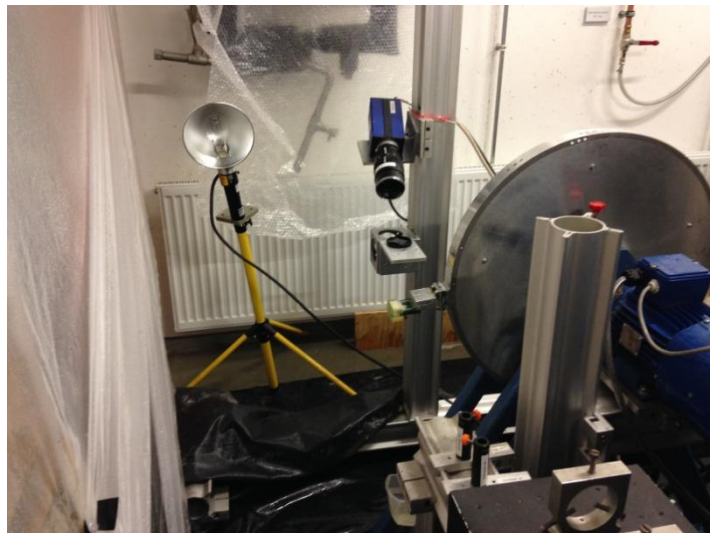


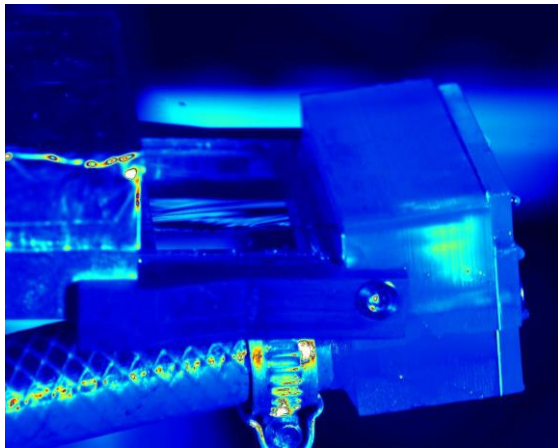
Figure 48: Position of the lamp and camera

The recordings of the paddle at the rotating flywheel have been made for three different Weber numbers: 4177, 7292 and 9854. The flow rate has been increased till 2.0 l/min starting at 0.3 l/min. The flow rate is increased by steps of 0.1 l/min till 1.4 l/min and then by steps of 0.2 l/min till 2.0 l/min. In Fig. 49 the most important results have been given.

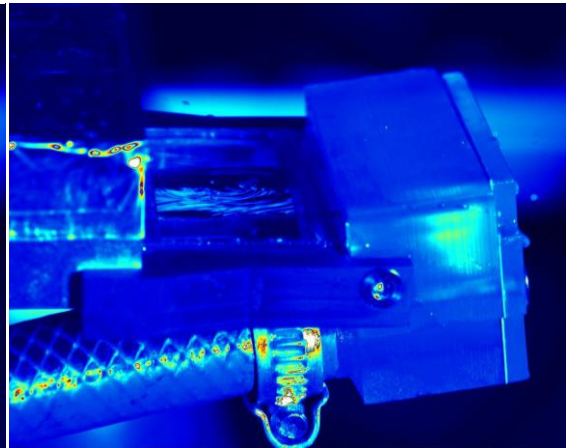
The results of the lowest Weber number, 4177, show that the film is still attached at a flow rate of 0.3 *l/min*. The film has waves at the sides but in the middle the flow is still smooth. However this changes very soon, at a flow rate of 0.4 *l/min*. This can be seen in the two top pictures of Fig. 49. The flow shows fluctuations. It is clearly that the film at this point becomes turbulent.

The two higher Weber numbers of 7292 and 9854 show that the film is already turbulent at a flow rate of 0.3 *l/min*. The amount of splashing here shows that the film also begins to separate from the glass plate. The two pictures of 2.0 *l/min* show a fully turbulent film which separates from the glass plate.

We 4177, 0.2 mm

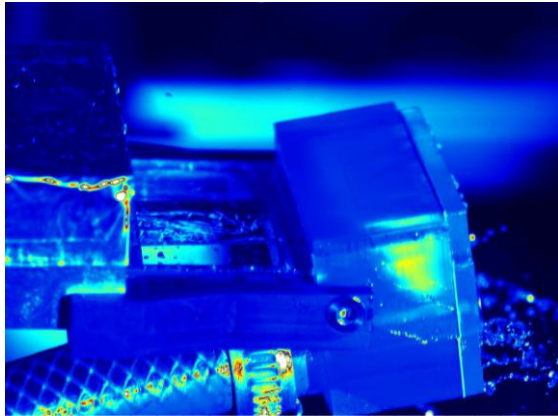


0.3 l/min

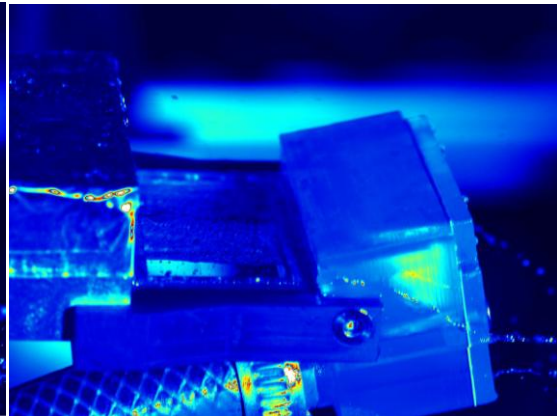


0.4 l/min

We 7292, 0.2 mm

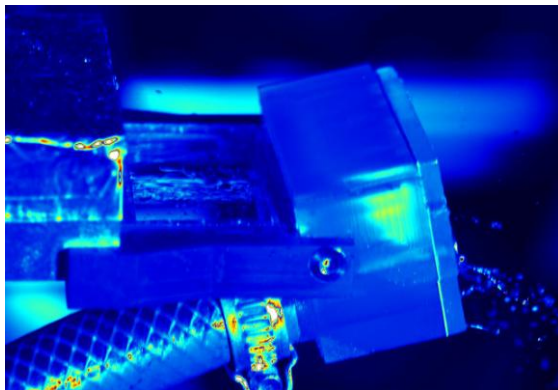


0.3 l/min

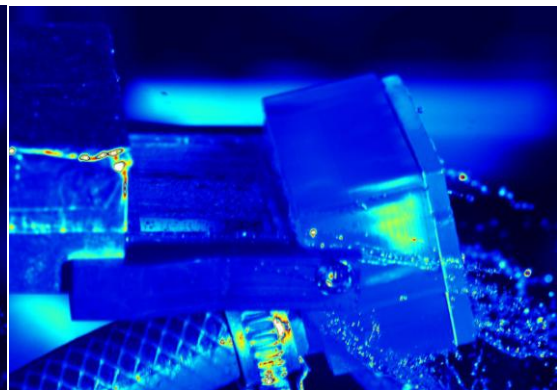


2.0 l/min

We 9854, 0.2 mm



0.3 l/min



2.0 l/min

Figure 49: Results experiment B, rotational flywheel

2.5.3. Discussion

The results of the geometry designed by Rohwedder showed flow separation at Weber numbers of 5826 and 5106 for respectively 0.1 mm and 0.3 mm. This happens at respectively a flow rate of 1.0 l/min and 0.75 l/min. In the research of this report a slit height of 0.2 mm was tested because no research had been done with this slit height thus far. The geometry tested, geometry 4, showed already turbulence at a flow rate of 0.4 l/min and a Weber number of 4177 with a slit height of 0.2 mm. This could have different causes. One possible cause is the arise of dirt in the geometry outlet. For this problem to be solved, first however the dirt should be further researched. Another possible cause is the connection of the geometry to the glass plate. Especially at higher flow rates an additional flow under the metal plates could be observed. This additional flow influenced the stability of the film. This could not be solved by simply tightening the geometry to the glass plate because then the glass plate could break. In the future the area under the sides of the geometry could be made not out of glass. In this way the water would still flow over the glass plate but the geometry could be tightened more to the surface. Another cause could be the slit height of the geometry outlet which was taken to be 0.2 mm, this will be further discussed in section 3. The increase of the Weber number till approximately 10000 results in the film being fully turbulent. Despite the better flow qualities of geometry 4 in the static research done in experiment A, this is worse than the results for the other slit heights and geometry. This makes clear that the height of the slit of geometry-outlet has a big influence on the stability of the film. During the experiment different problems arose, these will be briefly discussed below.

Problems

- The experiment with the rotating flywheel wasn't done with the original set-up as described in section 2.5.1. The problem was the use of the laser. The laser wasn't the same laser as in the experiment from V. Rohwedder [28]. The Brilliant laser used needs a constant signal from the light barrier. Otherwise the triggering process is not working. The Litron laser that was used in the earlier experiments is not that sensitive to variations in the signal. Therefore the laser was replaced by a stroboscope, Fig. 47. This flash light can replace the light source. The pulse of the stroboscope was manually adjusted with the frequency generator to give a pulse at the right moment. This set-up has eventually been used to get the results. Extra care was taken that no person was in the way of the light bundle because of the high power of the stroboscope.
- In the static situation again dirt has been observed in the slit of the canal.
- In the pictures another problem is observed. The outlet of the paddle is twisting at the two higher Weber numbers of 7292 and 9854. This could be another cause of the high splashing next to the flow separation.
- As can be seen in Fig. 49 the pictures are not completely zoomed at the whole film, but only at the front side. It appeared to be very difficult to get the whole film in the picture.
- The position of the water jet pump has been changed with respect to the set-up of experiment A. The new set-up can be seen in Fig. 50.



Figure 50: New position of the water jet pump

The new position lifts the water jet pump a little bit to get the kink out of the hose connecting the pump to the water jet pump. The water jet pump had, despite this little lift, enough power to suck the water up from the paddle.

3. Evaluation and recommendations

In experiment A the geometry with the best film qualities was chosen. This was done without any measuring device. In experiment B this geometry, geometry 4 Fig. 24, was tested with a rotation of the flywheel up to approximately a Weber number of 10000. This geometry was compared with the geometry designed by Rohwedder because this report is in fact a continuation of the research of Rohwedder [28]. Geometry 4 showed worse results, in terms of turbulence, than the geometry designed by Rohwedder. However the geometry of Rohwedder was tested with a slit height of 0.1 and 0.3 mm and geometry was tested with a slit height of 0.2 mm. Comparison between the two geometries with the same slit height of 0.2 mm only has been done in the static experiment, experiment A. Geometry 4 then had a better result than the old geometry, geometry 2. It is thus important that these geometries will be compared with each other at the same slit height in the flywheel experiment to take exact conclusions. Due to time issues this could not be done. The disappointing results of the film flow of geometry 4 could have had different reasons. During the static experiment several times dirt had been found in the slit of the geometry. Also the finishing of the printed polymer geometry showed problems. It was difficult to make a waterproof connection between the metal plates and the underside of the geometry. If the geometry was tightened too hard to the metal plates, the glass plate could break. Recommended is to fabricate new models with CNC-milling because then the finishing of the surfaces is more controlled. The analysis of the film has been done by analyzing the recordings. In the future it is recommended that equipment should be used to measure the film height for a better analysis of the behavior of the film flow.

The failure of the new geometry could be demonstrated by the analysis of Fig. 22. The critical Reynolds number of 313, equation 2.10, gives a border and the Weber number of 10000 gives a border. In the area that is formed by those two borders, the characteristic of a slit height of 0.1 mm is situated. Recommended is, to compare the old geometry 2 with the new geometry 4 with a slit height of 0.1 mm.

Personal note

During the internship I have learnt to combine theory with praxis. It is something that I didn't do before in this scale. First a theoretical research will be done and then a validation of your findings with a practical approach. Afterwards the coupling of theory with praxis has been done. Somewhat I still find it hard to do this in this context. There are very much results that should be combined into a conclusion. Things that could have been done better are the planning and the combining of my results. Next time I should make a better planning of the exact things that I want to measure. The results should be archived better. In this way it is easier to get a good overview of the things that I want to compare with each other. Some results that I had couldn't be used very well because there was nothing to compare them with. Overall the internship has been a great experience, I have seen how the practical side of a research works.

References

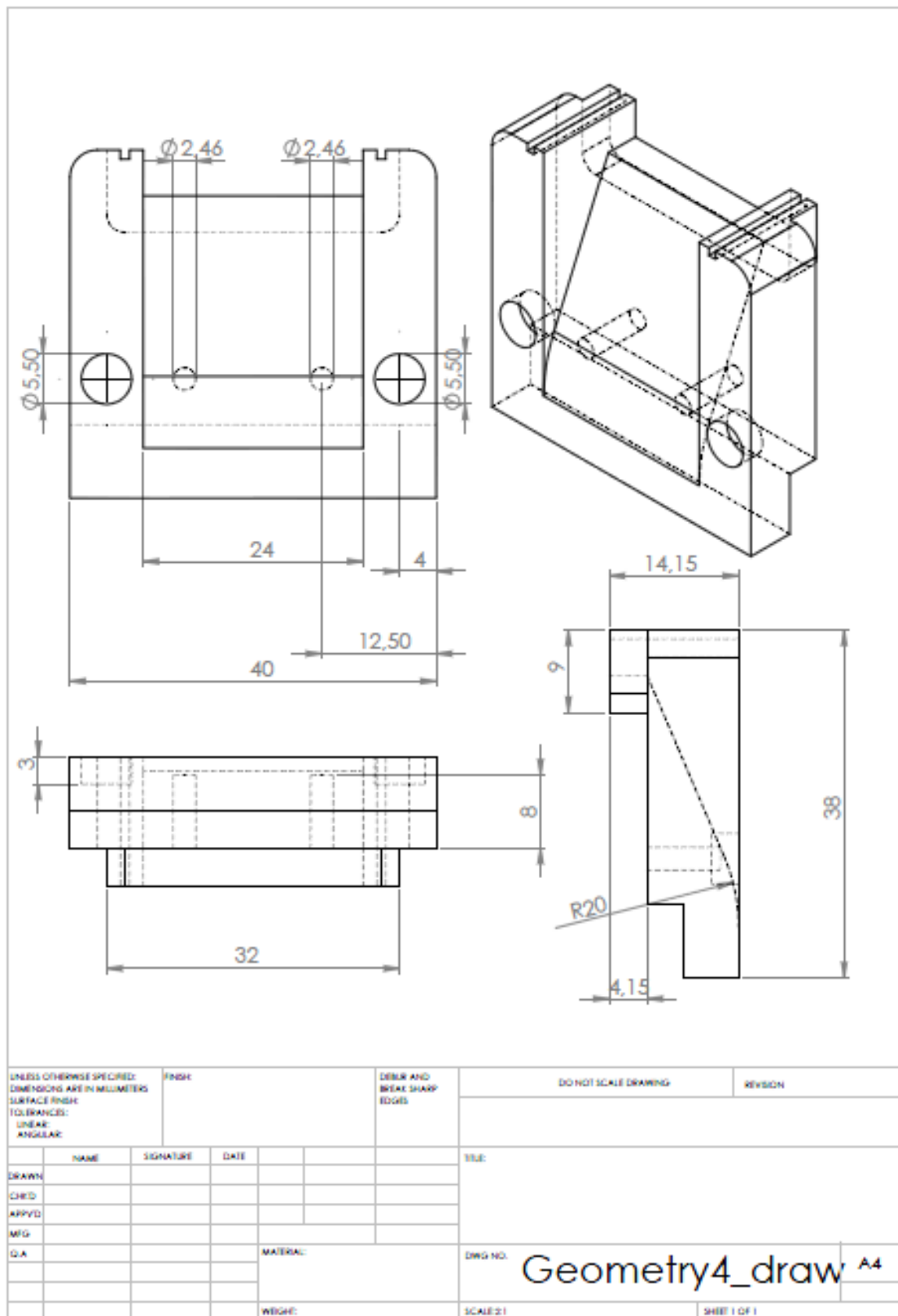
- [1] R. D. Deegan, P. Brunet, J. Eggers: *Complexities of splashing*. Nonlinearity, Series 21, C1-11 (2008)
- [2] R. Reske: *Experimentelle Untersuchung des Verhaltens frei fallender Wassertropfen beim Auftreffen auf dünnen Wasserfilmen*. Fortschrittsberichte VDI, series 7: Strömungstechnik, Nr. 115, Düsseldorf (1987)
- [3] H. E. Edgerton: *Stopping time: the photographs of Harold Edgerton* (Abrams: New York 1977)
- [4] D. H. Peregrine, *The fascination of Fluid Mechanics*. Journal of Fluid Mechanics, Volume 106, p. 59 (1981)
- [5] S. T. Thoroddsen, *The ejecta sheet generated by the impact of a drop*. Journal of Fluid Mechanics, Volume 451, p.373 (2002)
- [6] R. L. Vander Wal, J. P. Kizito, G. Tryggvason, G. M. Berger, S. D. Mozes: *Droplet-Surface Impingement Dynamics for Intelligent Spray Design*. NASA/TM-2004-213114 (2004)
- [7] B. W. Faßmann, S. E. Bansmer, T. J. Möller, R. Radespiel, M. Hartmann: *High velocity impingement of single droplets on a dry smooth surface*. Experiments in Fluids, Volume 54, Series 1516 (2013)
- [8] H. Schlichting, K. Gersten: *Grenzschicht-theorie*. Springer-verlag, Berlin Heidelberg, 10. Edition (2006)
- [9] G. F. Dietze: *Flow separation in falling liquid films*. Dissertation, Sierke Verlag, Göttingen, 1. Edition (2010)
- [10] A. Alhelfi: *Heat transfer in liquid film over the surface of a rotating disk subjected to impinging jet*. Project report, Lund University Sweden (2012)
- [11] V. M. Rohwedder: *Experimentelle Untersuchung des benetzten Tropfenaufpralls bei hohen Weberzahlen*. Diploma thesis, Technische Universität Braunschweig, Equation 3.18 (2014)
- [12] D. E. Hartley, W. Murgatroyd: *Criteria for the Break-Up of Thin Liquid Layers Flowing Isothermally Over Solid Surfaces*. International Journal of Heat and Mass Transfer, Volume 7, S. 1003-1015 (1964)
- [13] http://dodo.fb06.fh-muenchen.de/herberg/texte/mikronanotechnik/vass/kap4_1.pdf
- [14] H. Brauer: *Grundlagen der Einphasen- und Mehrphasenströmungen*. Verlag Sauerlander, Frankfurt am Main, 1. Edition (1971)
- [15] V. M. Rohwedder: *Experimentelle Untersuchung des benetzten Tropfenaufpralls bei hohen Weberzahlen*. Master thesis, Technische Universität Braunschweig, Equation 3.39 (2014)
- [16] Y. X. Su: *Flow Analysis and Design of Three-Dimensional Wind Tunnel Contractions*. American Institute of Aeronautics and Astronautics Journal, Volume 29, NO. 11 (1991)
- [17] T. Morel: *Comprehensive Design of Axisymmetric Wind Tunnel Contractions*. Journal of Fluids Engineering, ASME Transactions, Series 1, Volume 97, p. 225-233 (1975)

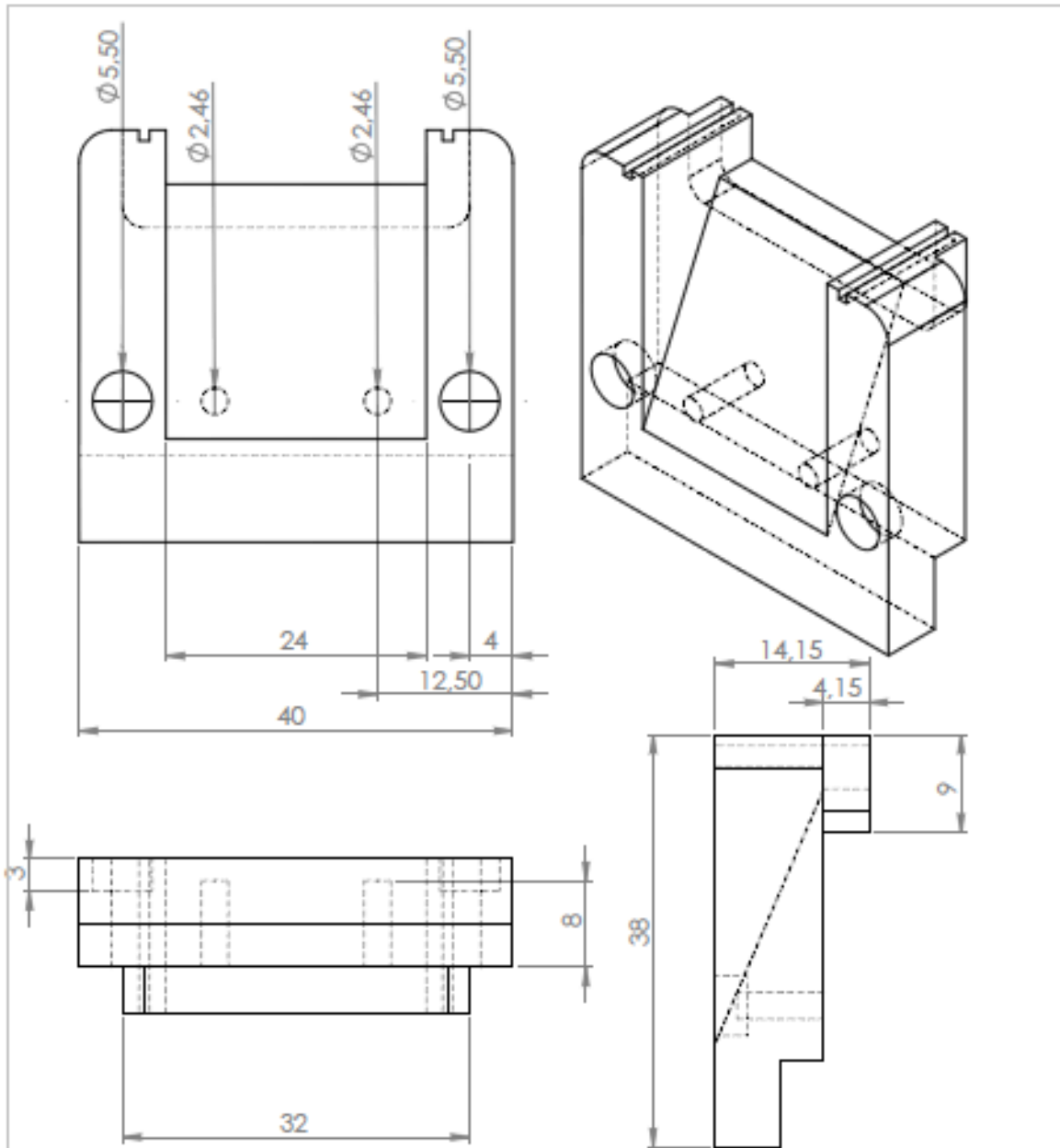
- [18] H. Fujimoto, Y. Suzuki, T. Hama, H. Takuda: *Flow Characteristics of Circular Liquid Jet Impinging on a Moving Surface Covered with a Water Film*, ISIJ International, Volume 51, No. 9, p. 1497–1505 (2011)
- [19] V. T. Chow: *Open-Channel Hydraulics*. International student edition, McGraw-Hill Book Company, p. 164-165 (1959)
- [20] V. M. Rohwedder: *Experimentelle Untersuchung des benetzten Tropfenaufralls bei hohen Weberzahlen*. Master thesis, Technische Universität Braunschweig, p. 81 (2014)
- [21] V. M. Rohwedder: *Experimentelle Untersuchung des benetzten Tropfenaufralls bei hohen Weberzahlen*. Master thesis, Technische Universität Braunschweig, p.70 (2014)
- [22] V. M. Rohwedder: *Experimentelle Untersuchung des benetzten Tropfenaufralls bei hohen Weberzahlen*. Master thesis, Technische Universität Braunschweig, p. 98 (2014)
- [23] <http://www.thermopedia.com/content/1117/>
- [24] V. M. Rohwedder: *Experimentelle Untersuchung des benetzten Tropfenaufralls bei hohen Weberzahlen*. Master thesis, Technische Universität Braunschweig, p. 109 (2014)
- [25] S. E. Bansmer: *Lecture Multiphase flow*. Institute of Fluid Mechanics, Technische Universität Braunschweig, April 2014
- [26] <http://theartreserve.com/harold-edgerton-milk-drop-coronet-1957/>
- [27] A. L. Yarin, D. A. Weiss: *Impact of drops on solid surfaces: Self similar capillary waves, and splashing as a new type of kinematics discontinuity*. Journal of Fluid Mechanics, Volume 283, p. 141-173 (1995)
- [28] V. M. Rohwedder: *Experimentelle Untersuchung des benetzten Tropfenaufralls bei hohen Weberzahlen*. Master thesis, Technische Universität Braunschweig (2014)
- [29] J. D. Anderson: *Fundamentals of aerodynamics*. McGraw-Hill Book Company, New York, 5. Edition (2011)

Appendices

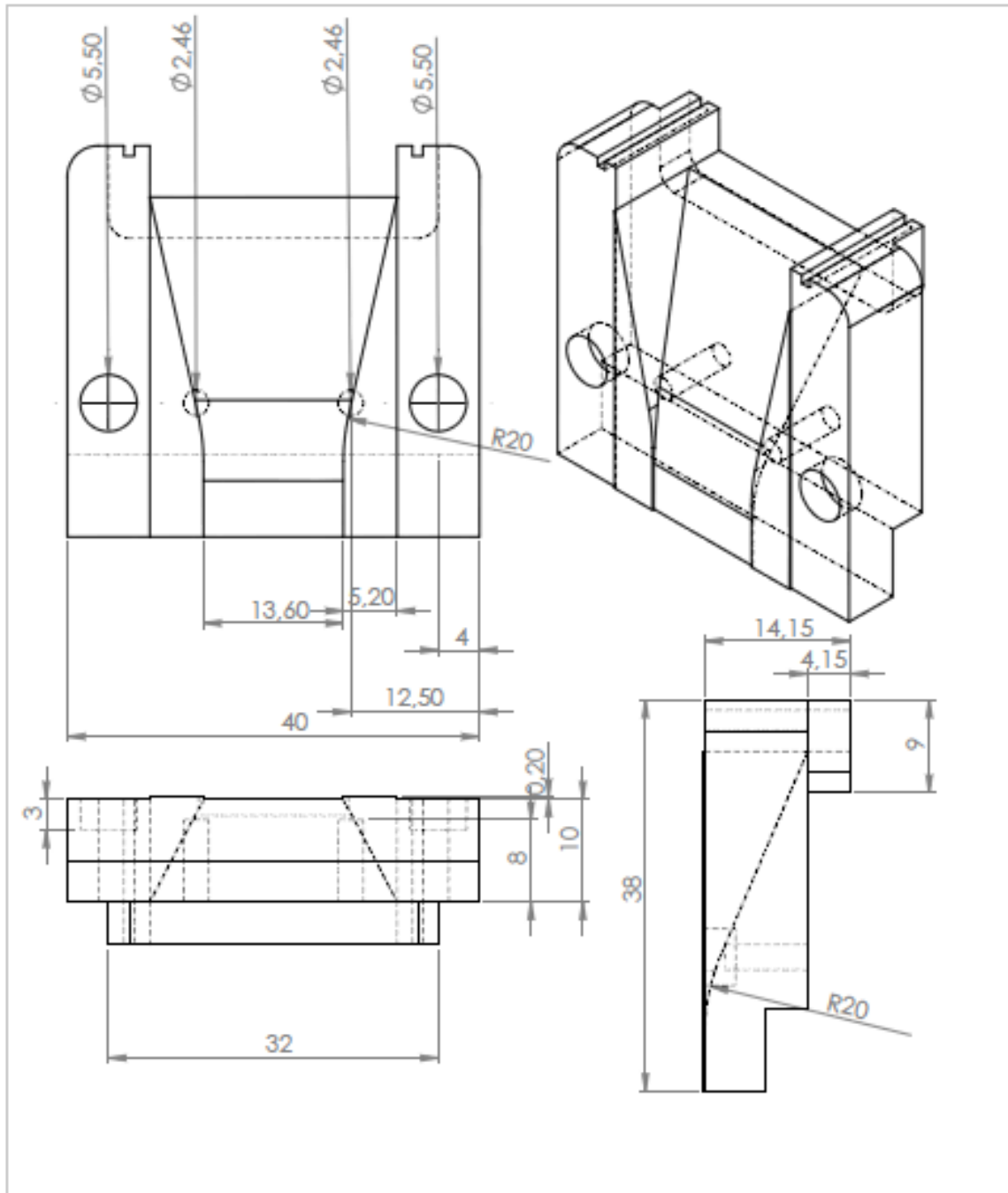
- Appendix A: Solidworks drawings of the designed geometries
- Appendix B: Material list for experiment B

Appendix A

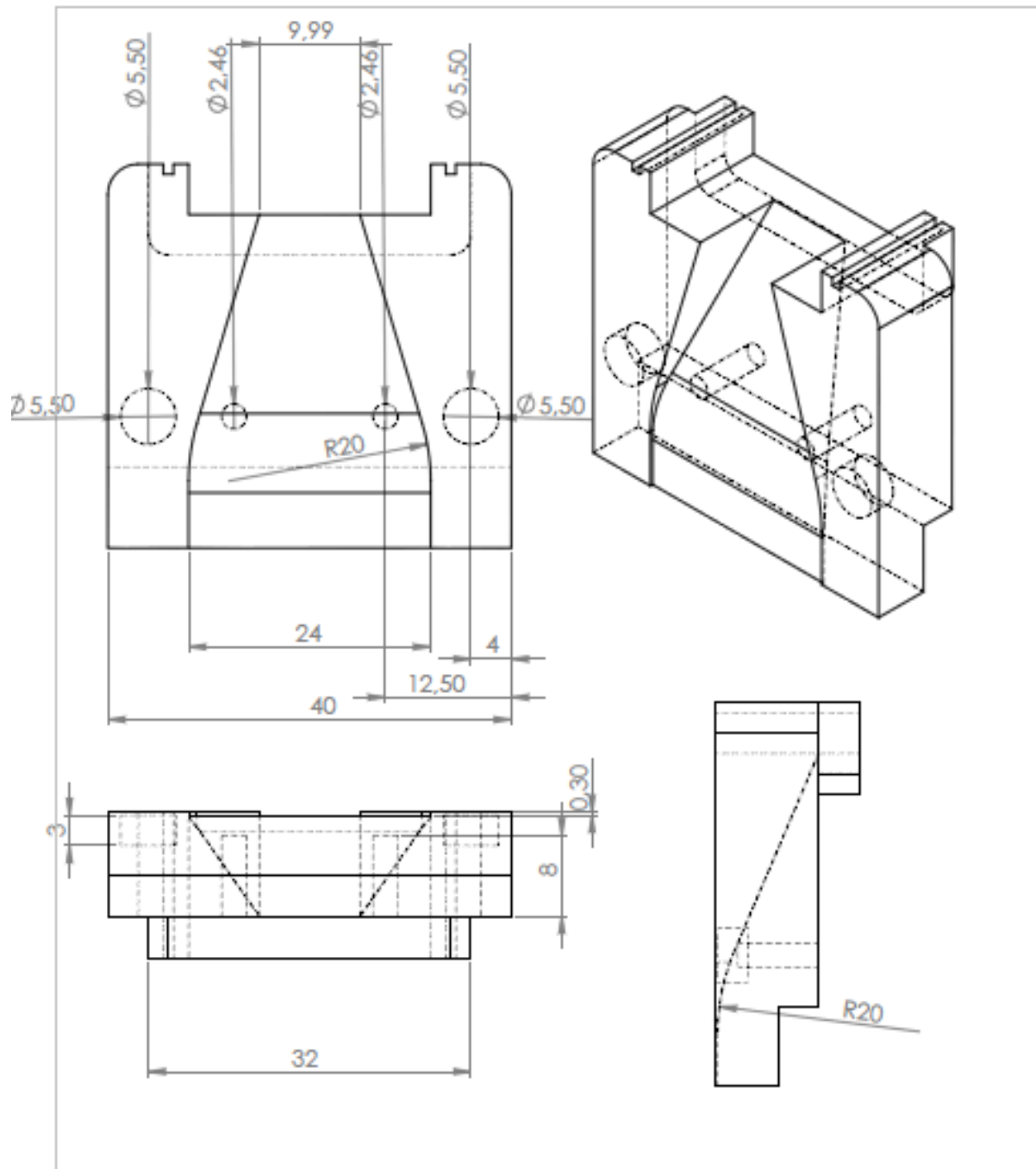




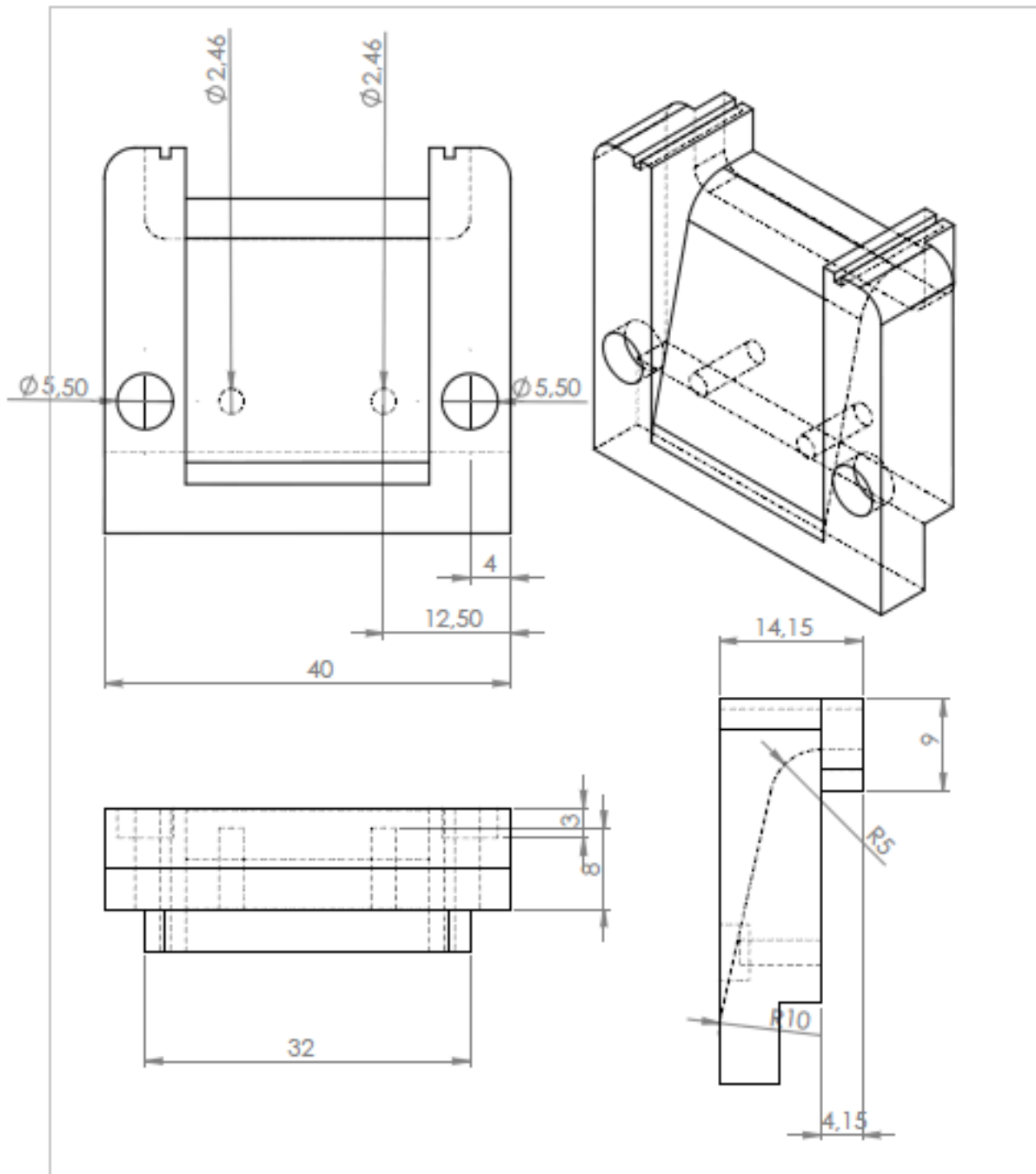
UNLESS OTHERWISE SPECIFIED: DIMENSIONS ARE IN MILLIMETERS SURFACE FINISH: TOLERANCES: LINEAR: ANGULAR:				FINISH:	DEBUR AND BREAK SHARP EDGES	DO NOT SCALE DRAWING	REVISION
NAME	SIGNATURE	DATE				TITLE:	
DRAWN						DWG NO. Geometry5_draw A4	
CHECK						SCALE: 2:1	SHEET 1 OF 1
APPROVED							
MFG							
Q.A.					MATERIAL:		
					WEIGHT:		



UNLESS OTHERWISE SPECIFIED: DIMENSIONS ARE IN MILLIMETERS SURFACE FINISH: TOLERANCES: LINEAR: ANGULAR:				FINISH	DEBUR AND BREAK SHARP EDGES	DO NOT SCALE DRAWING	REVISION
NAME	SIGNATURE	DATE				TITLE	
DRAWN							
CHEK							
APPVD							
MFG							
D.A.				MATERIAL:		DWG NO.	Geometry6_draw A4
				WEIGHT:		SCALE: 2:1	SHEET 1 OF 1



UNLESS OTHERWISE SPECIFIED: DIMENSIONS ARE IN MILLIMETERS SURFACE FINISH: TOLERANCES: LINEAR: ANGULAR:		FINISH:	DEBUR AND BREAK SHARP EDGES		DO NOT SCALE DRAWING	REVISION
DRAWN	NAME	SIGNATURE	DATE		TITLE:	
CHECKED						
APPROVED						
MFG						
Q.A.				MATERIAL:	DWG NO. Geometry7_draw A4	
				WEIGHT:	SCALE: 2:1	SHEET 1 OF 1



UNLESS OTHERWISE SPECIFIED: DIMENSIONS ARE IN MILLIMETERS SURFACE FINISH: TOLERANCES: LINEAR: ANGULAR:				FINISH	DEBUR AND BREAK SHARP EDGES	DO NOT SCALE DRAWING	REVISION
DRAWN	NAME	SIGNATURE	DATE			TITLE	
CHEK							
APPVD							
MFG							
QA					MATERIAL:	DWG NO.	Geometry8_draw A4
					WEIGHT:	SCALE: 2:1	SHEET 1 OF 1

Appendix B

Material list for experiment B

<i>Device</i>	<i>Type</i>
Motor of the flywheel	Ateg, EP 80 4A made by the ISM
High speed camera	LaVision GmbH, Imager pro 5
Laser	Brillant twint laser by quantel lasers pulsed Nd: YAG laser
PTU	La Vision GmbH
Lens	Carl Zeiss AG, Makro-Planar 2/50 mm ZF
Computer	-
Diffuser	LaVision GmbH
Universal counter	PeakTech® Prüf- und Messtechnik GmbH 2540, 1,5 GHz
Oscilloscope	Tektronix®, 2431L
Frequency generator	Hameg® Instruments GmbH, HM8131-2
Pump	WILO, WJ-202-X-EM/B
Water jet pump	Stübbe
Volume flow meter	Kobold